IL NUOVO CIMENTO Vol. ■■, N. ■ [redacted] 1987

Please send back these proofs as soon as possible in order to speed up the publication of the paper. Thanks

Original Proofs

Please [illegible] in 2 ex. the other set is for Author's convenience.

Low-Energy Muons in Extensive Air Showers (EAS).

D. K. BASAK

~~Department of Physics, University of North Bengal - Darjeeling-734 430, India~~
Department of Physics, A.C. College - Jalpaiguri, West Bengal 735 101, *India*

N. CHAUDHURI, S. SARKAR, B. BHATTACHARYA and B. GHOSH

Department of Physics, University of North Bengal - Darjeeling-734 430, *India*

(ricevuto il 18 Novembre 1986)

Summary. — A small air shower array of 21 detectors in conjunction with two shielded muon magnetic spectrographs has been operated for detection of muons of momentum in the range $(2 \div 500)$ GeV/c at a geomagnetic latitude of 26° 45′ N at North Bengal University Campus. The array is sensitive to air showers initiated by cosmic-ray primaries of energy in the range $(10^{14} \div 10^{16})$ eV. The initial results on muons with a comparison of other recent measurements have been made to infer information on the characteristics of high-energy interaction. An evaluation on the Monte Carlo simulation and observational data on muons in air showers has also been given to indicate the present status of the study of muons in air showers.

PACS. 94.40. – Cosmic rays.

1. – Introduction.

The on-going experiments with the shielded magnetic spectrographs and EAS array described in an earlier paper (1) are the source of stimuli for an evaluation of the simulation and observational air shower muon data accumulated in the last decade and a comparison with old data in the overlapping

(1) D. K. BASAK, N. CHAKRAVORTY, B. GHOSH, G. C. GOSWAMI and N. CHAUDHURI: *Nucl. Instrum. Methods*, **227**, 167 (1984).

range of experiments before 1985. In addition to two shielded muon magnetic spectrographs, a neon flash tube (NFT) chamber has also been used as a low-energy muon detector in the NBU air shower array. It consists of 9 layers of neon flash tubes installed in a chamber with a cover of 5 cm of lead and concrete shield of $\sim 1100\ g/cm^2$ to get rid of electron component. This NFT chamber helps to locate the trajectories of muons with an energy threshold at 1.5 GeV.

The measurement of muon distribution in EAS is very important because of its relevance to high-energy nuclear interaction processes as well as the nature of cosmic-ray primary particles.

2. – Experimental arrangement.

The NFT chamber used as muon detector covers on area of 1 m × 1 m for the localization of muon trajectories. The schematic diagram of the NFT chamber is shown in fig. 1. The two magnetic spectrographs (m.d.m. 500 GeV/c) under a concrete shielding absorber and with the provision of flash tube recording of muon trajectories have been described in detail by BASAK *et al.* [1]. The accuracy of locating a muon trajectory is within ± 0.14 cm.

Fig. 1. – *a*) The schematic diagram of neon flash tube chamber, *b*) arrangement of tubes and electrodes in each tray.

The NFT chamber and spectrographs were operated under an EAS trigger which was also used for recording the muon trajectories on photographic film. This experimental arrangement enabled to record muons at three different positions simultaneously. The details regarding the determination of muon momentum and m.d.m. of the spectrograph from the recorded trajectory are given in appendix A.

3. – Low-energy muon data and analysis.

A total of 2000 showers has been studied so far for the analysis of low-energy muons. Out of these 1505 showers have been found to be in the shower size range $1 \cdot 10^4 \div 4 \cdot 10^5$ particles and associated with muons in the NFT chamber.

3·1. *Measurement of muon density.* – The density of muons detected by NFT chamber at a particular distance is determined by the expression for the average muon density at a particular distance group for a given shower size group given as

$$\varrho_\mu(N_e, r, > E_\mu) = \frac{n_\mu(N_e, r)}{N_t(N_e, r) A'}, \tag{1}$$

where $n_\mu(N_e, r)$ is the total number of muons recorded in a particular distance interval (r) for particular shower size (N_e) in a certain period of time, $N_t(N_e, r)$ represents the total number of showers of size (N_e) at the distance interval (r) recorded at the same time and A' is the effective area of the flash chamber, that recorded the muons.

4. – Observed lateral distribution of muons in EAS.

At the particular distance from the shower core the average muon density is calculated by using formula (1). The observed lateral distribution of muons is shown in fig. 2 and 3 along with the distribution, according to the formulation of Greisen ([2]) for muon threshold energy around 1.5 GeV. The line represents the least-squares fit to the observed distribution.

Fig. 2. – Observed lateral distribution of muons ($E_\mu \geqslant 1.5$ GeV) in showers of size range $1.08 \cdot 10^4 \div 3.5 \cdot 10^4$ particles: o experimental points, – – – GREISEN ([2]).

Fig. 3. – Observed lateral distribution of muons ($E_\mu \geqslant 1.5$ GeV) in showers of size range $6 \cdot 10^4 \div 1 \cdot 10^5$ particles: o experimental points, – – – GREISEN ([2]).

Fig. 4. – Observed muon lateral distribution in EAS for $E_\mu \geqslant 1$ GeV and $N_e = 10^5$: o fitted points from experimental data ([3-6]), • GREISEN ([2]), ▵ TURVER ([7]), ▽ GRIDER ([8]), ◒ present experiment.

5. – A comparison of observed and simulated lateral distribution of muons in EAS.

Figure 4 shows an example of fitted results from the muon data obtained by DZIKOWSKI *et al.* ([3]), BONEZACK ([4]), VERNOV ([5]) and POPOVA ([6]) for all showers in the size range $2 \cdot 10^5 \div 5.6 \cdot 10^5$ particles observed at sea-level. The lowest energy of muons detected in these showers is around 1 GeV. The final distri-

([2]) K. GREISEN: *Annu. Rev. Nucl. Sci.*, **10**, 63 (1960).

([3]) T. DZIKOWSKI, R. FIRKOWSKI, J. GAWIN, W. OLEJNICZAK, S. PACHALA and J. WDOWCZYK: *Proceedings of the XIV International Conference on Cosmic Rays*, Vol. **8** (Munich, 1975), p. 2795.

([4]) B. BONEZACK, R. FIRKOWSKI, J. GAWIN, J. HIBNER, R. MAZE, J. WDOWCZYK and A. ZAWADZKI: *Proceedings of the X International Conference on Cosmic Rays*, Vol. **46** (Calgary, 1967), p. 102.

([5]) S. N. VERNOV, G. B. KHRISTIANSEN, O. V. VEDENEEV, N. N. KALMYKOV, G. V. KULIKOV, K. V. MANDRITSKAYA and V. I. SOLOVEVA: *Acta Phys. Acad. Sci. Hung.*, **29**, Suppl. 3, 429 (1970).

([6]) L. POPOVA: *Proceedings of the XV International on Cosmic Ray Conference*, Vol. **8** (Plovdiv, 1977), p. 403.

bution corresponding to the fitted data points is well represented by the function

$$\varrho_\mu(R) = K/R(n + aR), \tag{2}$$

where $K = 2.298$, $n = 0.5934$ and $a = 1.932 \cdot 10^{-3}$. The functional forms of muon lateral distribution for larger shower groups at all altitudinal levels are same as eq. (2) but with different parameters. The distribution function as given by GREISEN (2) along with simulation results by TURVER (7) and GRIEDER (8) for the corresponding shower size is indicated in the figure along with the present experimental points to show the present status of the observational and simulation muon data. The present status of calculated results by TURVER (7), GRIEDER (8), KANEKO *et al.* (9), DE BEER *et al.* (10), DEDENKO *et al.* (11), HILLAS (12) and GAISSER (13) on muon lateral distribution (normalized to $N_e = 10^6$) is shown in fig. 5 for muon threshold energy $\geqslant 1$ GeV.

Fig. 5. – Calculated results on muon lateral distribution at $E_\mu \geqslant 1$ GeV and $N_e = 10^6$: ▲ TURVER (7), ◒ GRIEDER (8), ○ KANEKO *et al.* (9), • DE BEER *et al.* (10), ▽ DEDENKO *et al.* (11), ▲ HILLAS (12), ◐ GAISSER (13).

6. – The muon energy spectrum.

The measurements using magnetic spectrographs of the integral energy spectrum of muons in air showers have been evaluated. There exists only two or three measurements at smaller core distances between 5 to 50 m in the showers of size range $3 \cdot 10^4 \div 1 \cdot 10^6$. The present measurements and the measurements of Moscow Group (14) do not agree with simulation results of Turver (7) but are consistent with the distribution of Greisen (2) (fig. 6).

(7) K. E. TURVER: private communication (1980).
(8) P. K. F. GRIEDER: *Nuovo Cimento*, **7**, 1 (1977).
(9) T. KANEKO, C. AGUIRRE, Y. TOYODA, H. NAKATANI, S. JADOT, P. K. MACKEOWN, K. SUGA, F. KAKIMOTO, Y. MIZUMOTO, K MURAKAMI, K. NISHI, M. NAGANO and K. KAMATA: *Proceedings of the XIV International Conference on Cosmic Ray*, Vol. **8** (Munich, 1975), p. 2747.
(10) J. F. DE BEER, B. HOLYOAK, H. ODA, J. WDOWCZYK and A. W. WOLFENDALE: *J. Phys.*, **46**, S737 (1968).
(11) L. G. DEDENKO and G. B. KHRISTIANSEN: *Proceedings of the XV International Conference on Cosmic Ray*, Vol. **8** (Plovdiv, 1977), p. 474.
(12) A. M. HILLAS: *Proceedings of the IX International Conference on Cosmic Ray*, Vol. **2** (London, 1965), p. 758.
(13) T. K. GAISSER: private communication (1980).
(14) N. V. GRISHINA, YU. A. FOMIN, A. P. LEBEDEV, N. N. KALMYKOV, B. A. KHRENOV, G. B. KHRISTIANSEN, G. V. KULIKOV, S. M. ROZHDESTVENSKY, A. A. SILAEV, V. I. SOLOVJEVA, A. P. SULAKOV and Z. V. YAROCHKINE: *Proceedings of the XVII International Conference on Cosmic Ray*, Vol. **6** (Paris, 1981), p. 3.

Fig. 6. – Comparison of muon energy spectrum: Moscow Group [14]: ▵ ($r = 5$ m), ▿ ($r = 12$ m), ○ ($r = 24$ m), TURVER [7] – – – ($r = 12$ m), – · – · – ($r = 24$ m), GREISEN [2] ———, present experiment: ◒ ($r = 5$ m), ▲ ($r = 12$ m), • ($r = 22.8$ m).

7. – Variation of muon density with shower size.

In the shower size range of $1 \cdot 10^4 \div 4 \cdot 10^5$ particles the results on the variation of muon density as a function of shower size are shown in fig. 7 which are similar to those calculated by CHATTERJEE *et al.* [15] and SAMORSKI and STAMM [16].

Fig. 7. – Variation of observed density ($E_\mu \geqslant 1.5$ GeV) with shower size: • ($r = 7.5$ m), ▵ ($r = 16$ m), ◒ ($r = 24$ m), ○ ($r = 40$ m).

Using the form

$$\varrho_\mu(r) \propto N_e^\beta .$$

We have calculated the exponent (β) by fitting the observed data. A comparison of exponents obtained by other authors [15,16] is given in table I for various shower size ranges and core distances.

TABLE I.

Shower size range	Core distance (m)	Values of exponent (β)	Authors
$10^5 \div 2 \cdot 10^7$	20	0.75 ± 0.15	CHATTERJEE *et al.* [15]
$10^5 \div 10^7$	10	0.74 ± 0.07 0.94 ± 0.11	SAMORSKI and STAMM [16]
$2.64 \cdot 10^4 \div 2 \cdot 10^5$	16	0.864	present experiment
$2.64 \cdot 10^4 \div 2 \cdot 10^5$	40	0.904	present experiment

8. – Conclusion.

We note that the various simulation data on muons in air showers differ and there is disagreement between simulations and observations on showers in the size range $10^5 \div 10^8$ particles.

---

[15] B. K. CHATTERJEE, N. V. GOPALAKRISHNAN, G. T. MURTHY, S. NARAYAN, B. V. SRIKANTAN, M. V. SRINIVASA RAO, S. T. TONWAR and R. H. VATCHA: *Can. J. Phys.*, **46**, S131 (1968).

[16] M. SAMORSKI and W. STAMM: *Proceedings of the XVIII International Conference on Cosmic Rays*, Vol. **11** (Bangalore, 1983), p. 244.

The lateral distribution of muons for each of the various size groups has the same dependence on radial distance and the discrepancy between the calculated (7) and observed distributions increases with radial distance. The Monte Carlo simulation results of Turver (7) are based on scaling model with constant cross-section for high-energy nuclear interaction. The present study shows that these assumptions about high-energy nuclear interaction have to be changed to see if there is any effect on the muon distributions in EAS for the same primary mass values. The measured and the calculated muon energy distributions are inconsistent. Some of the calculated results on muon lateral distribution published in the seventies are mutually inconsistent. Present measurements on muon lateral distribution and energy spectrum in air shower with magnetic spectrograph show that there is agreement with the experimental results by other workers. The variation of muon density as a function of shower size shows good agreement with the results by other groups.

APPENDIX A

Calculation of momentum of muon recorded by the magnetic spectrograph.

A particle of momentum p and charge e, is moving transversely through a magnetic field of induction B is related to the radius of curvature ϱ of its path given by

$$p = 300 B\varrho \ (\mathrm{eV/c}) , \tag{A.1}$$

where p (eV/c) is the momentum of the particle, ϱ (cm) is the radius of curvature of the path. If dl be the length of the element of path traversed by the particle normal to the field and $d\varphi$ be the deflection of the particle due to magnetic field, then

$$\varrho = \frac{dl}{d\varphi} .$$

Neglecting energy loss in material of the magnet, the momentum of the particle can be written as

$$p = \frac{300 \int B \, dl}{\varphi} \ (\mathrm{eV/c}) , \tag{A.2}$$

where B is in G, l is in cm and φ in radians.

A schematic diagram of the magnetic spectrograph along with the particle trajectory is shown in fig. 8. The deflection in the magnetic field is calculated

Fig. 8. – A schematic diagram of the magnetic spectrograph along with the particle trajectory.

from the four measured co-ordinates along the length of the trajectory. FT_1, FT_2, FT_3 and FT_4 are four neon flash tube trays which determine the particle trajectory. The reference line $ACEG$ is at a distance a_0, b_0, c_0, d_0 from the four flash tube trays (FT_1, FT_2, FT_3, FT_4), respectively. CL is the central line of the magnetic spectrograph and the effective length of the magnet is $2L$, where $2L = 106.3$ cm. x_1 and x_2 are the distance of the trays as shown in fig. 8 and $x_1 = 31.85$ cm, $x_2 = 85$ cm, $L + x_1 = x_2 = 85$ cm.

If a perpendicular is drawn from H' on EF', we get from the geometry of the particle trajectory

$$\frac{GH' - EF'}{\overline{FT_3 \cdot FT_4}} = \frac{CD - AB}{\overline{FT_1 \cdot FT_2}} .$$

Now,

$$\frac{GH + HH' - (EF + FF')}{\overline{FT_3 \cdot FT_4}} = \frac{CD - AB}{\overline{FT_1 \cdot FT_2}} \tag{A.3}$$

and

$$HH' = \varphi(L + x_1 + x_2) , \qquad FF' = \varphi(L + x_1) ,$$

$$GH' - EF' = (d + d_0) + \varphi(L + x_1 + x_2) - (c + c_0) - \varphi(L + x_1) = \varphi x_2 + (d + d_0) - (c + c_0) .$$

Since φ is the deflection at the central place of the magnet M. Hence

$$FT_1 \cdot FT_2 = FT_3 \cdot FT_4 .$$

Therefore from eq. (A.3), we get

$$\varphi x_2 + (d + d_0) - (c + c_0) = (b + b_0) - (a + a_0) ,$$

$$\varphi = \frac{[(b + b_0) - (a + a_0)] + [(c + c_0) - (d + d_0)]}{x_2} .$$

Now we can write

$$\varphi = \frac{\Delta_0 + \Delta_m}{x_2} = \frac{\Delta}{x_2} , \tag{A.4}$$

where

$$\Delta_0 = (b_0 - a_0) + (c_0 - d_0)$$

and

$$\Delta_m = (b - a) + (c - d) .$$

The quantity Δ_0 is the geometrical constant of the magnetic spectrograph and Δ_m is the geometrical constant due to magnetic deflection. From eqs.

(A.2) and (A.4) we have

$$p = \frac{300 \int B\,dl}{q}$$

$$= \frac{300\,B(2L)}{\Delta/x_2}$$

$$= \frac{300\,B \times 2L \times (x_2)}{\Delta} = \frac{C}{\Delta}\ (\mathrm{eV}/c)\,,$$

where $C = 300\,B \times (2L) \times x_2$.

For NBU magnetic spectrograph,

$$B = 1.62 \cdot 10^4\ \mathrm{G}\,, \quad 2L = 106.3\ \mathrm{cm}\,, \quad x_2 = 85\ \mathrm{cm}\,,$$

$$C = \frac{300 \times 1.62 \cdot 10^4 \times 106.3 \times 85}{1.999}\ (\mathrm{eV}/c)\ (\mathrm{t.s.})$$

and

$$p = \frac{21.96}{\Delta}\ (\mathrm{GeV}/c)\,, \tag{A.5}$$

where Δ is in t.s. unit (1 t.s. $= (1.999 \pm 0.002)$ cm).

The momentum can be calculated from eq. (A.5) by measuring the quantity Δ which can be written as

$$\Delta = \Delta_0 + \Delta_m\,,$$

where

$$\Delta_0 = (b_0 - a_0) + (c_0 - d_0)\,,$$

$$\Delta_m = (b - a) + (c - d)\,.$$

The values of a_0, b_0, c_0, d_0 are measured from the alignment of the spectrograph and a, b, c, d from the analysis of the spectrograph data obtained for each accepted event.

Equation (A.5) is used for the calculation of momentum of a particle passing through the magnetic spectrograph.

Appendix B

Calculation of maximum detectable momentum (m.d.m.) **of the spectrograph.**

The m.d.m. of the spectrograph is the momentum which corresponds to deflection equal to the error in the measurement of the deflection.

The co-ordinates (x_{ab}, x_{cd}) of intersection of particle trajectory at the central line of the spectrograph are given by

$$x_{ab} = b + \left(\frac{x_1 + L}{x_2}\right)(b - a) - (x_0 - b_0) + \left(\frac{x_1 + L}{x_2}\right)(b_0 - a_0) ,$$

$$x_{cd} = c + \left(\frac{x_1 + L}{x_2}\right)(c - d) - (x_0 - c_0) + \left(\frac{x_1 + L}{x_2}\right)(c_0 - d_0) .$$

Now the discrepancy at the central line of the magnetic spectrograph is given by

$$\varepsilon = x_{ab} - x_{cd} . \tag{B.1}$$

For high-energy particles the contribution of error to ε is small from multiple Coulomb scattering, whereas in the calculation of m.d.m. of the spectrograph, the track-location error is the only source of error to ε.

Assuming the existence of equal errors σ_i in the location of particle track in all the four arrays of the neon-flash tube trays the standard error in deflection Δ is given by

$$\sigma_\Delta = 2\sigma_i . \tag{B.2}$$

Now from eq. (B.1) we have

$$\begin{cases} \sigma_\varepsilon^2 = 2\sigma_i^2 \left[\left(\dfrac{x_1 + L}{x_2}\right)^2 + \left(1 + \dfrac{x_1 + L_1}{x_2}\right)^2\right] = 2\sigma_i^2 [1 + 4] , \\ \sigma_\varepsilon = \sqrt{10}\,\sigma_i . \end{cases} \tag{B.3}$$

From eqs. (B.2) and (B.3) we get

$$\sigma_\Delta = \frac{2}{\sqrt{10}}\,\sigma_\varepsilon .$$

The m.d.m. of the spectrograph is the momentum which corresponds to a deflection equal to the error in the deflection.

$$p_{\text{m.d.m.}} = \frac{C}{\sigma_\Delta} . \tag{B.4}$$

It can also be defined as the momentum which corresponds to the deflection equal to the most probable error ($0.6745\sigma_\Delta$) on the measured deflection and is given by

$$p_{\text{m.d.m.}} = \frac{C}{0.6745\sigma_\Delta} = \frac{C}{0.6745 \times (2/\sqrt{10})\,\sigma_\varepsilon} = \frac{21.96}{0.4266\,\sigma_\varepsilon}\ (\text{GeV/c}) . \tag{B.5}$$

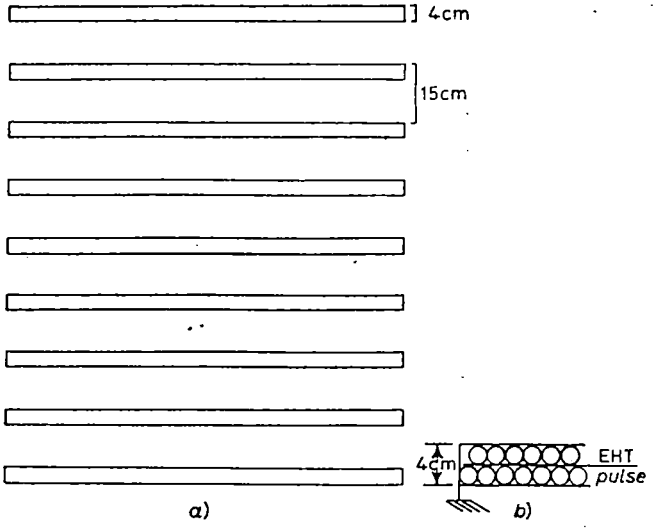
4cm
15cm
4cm
EHT
pulse
a)
b)

Fig. 1

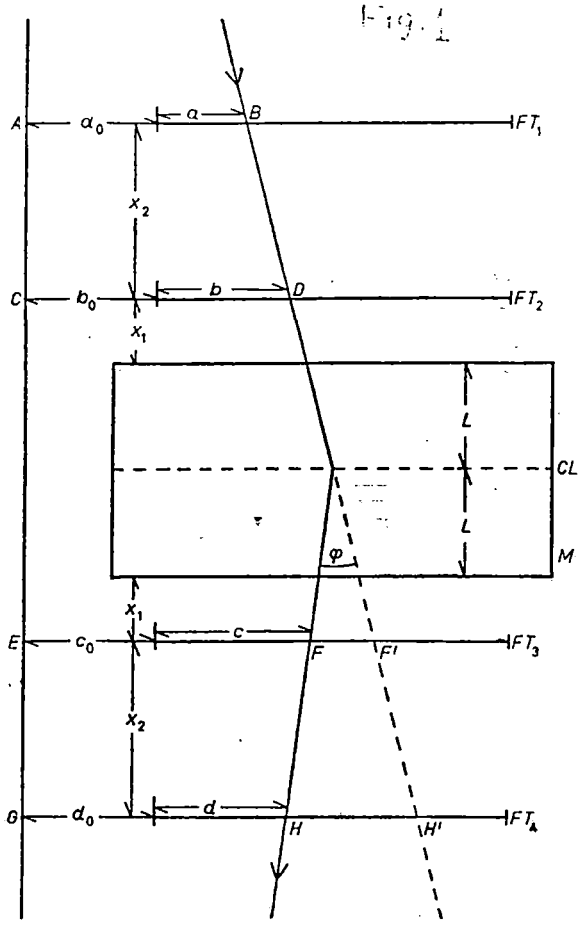
A
a_0
a
B
FT_1
x_2
C
b_0
b
D
FT_2
x_1
L
CL
L
M
φ
x_1
E
c_0
c
F
F'
FT_3
x_2
G
d_0
d
H
H'
FT_4

Fig. 8

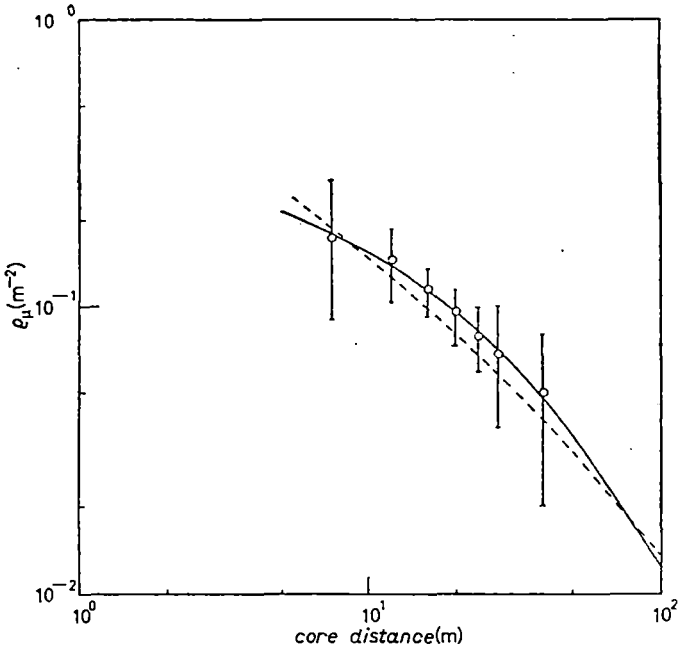
10^0
$\rho_\mu(m^{-2})$
10^{-1}
10^{-2}
10^0
10^1
10^2
core distance(m)

Fig. 2

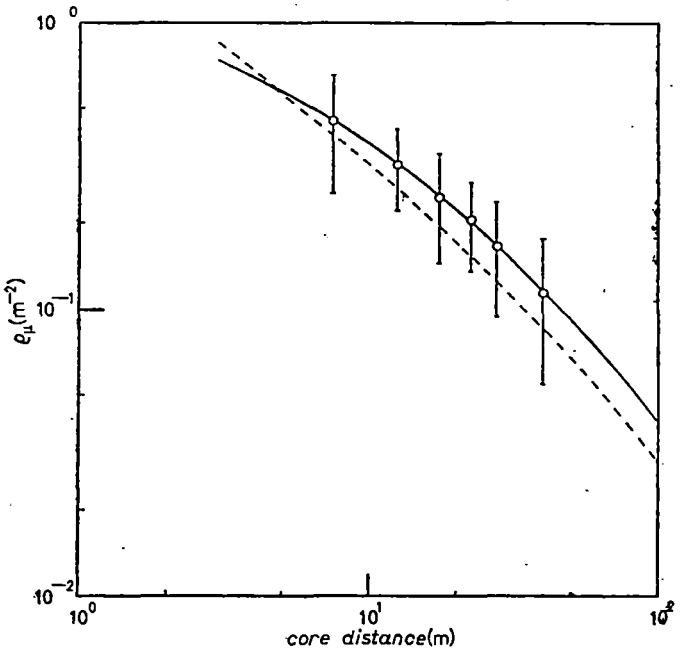
10^0
$\rho_\mu(m^{-2})$
10^{-1}
10^{-2}
10^0
10^1
core distance(m)

Fig. 3

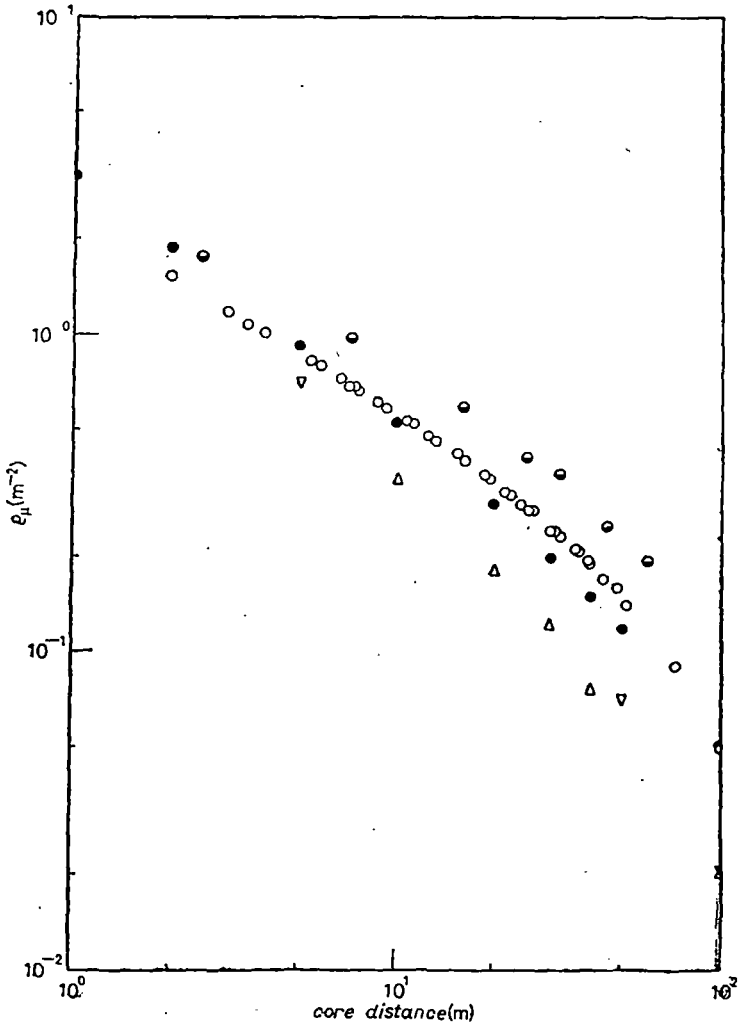

Fig. 4

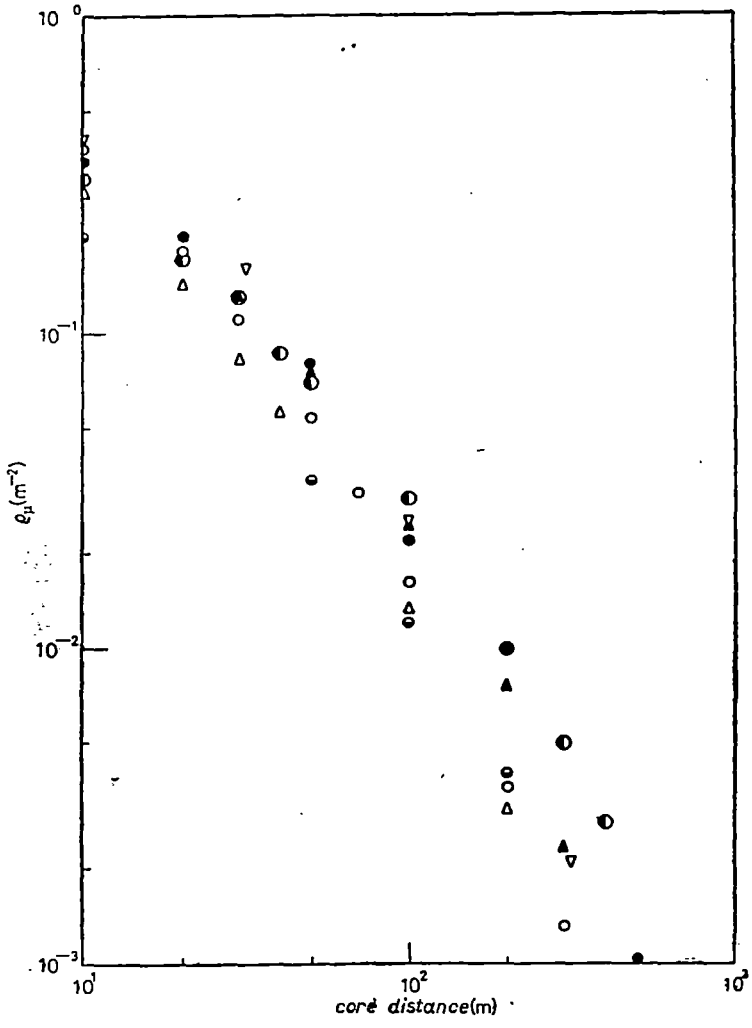

Fig. 5

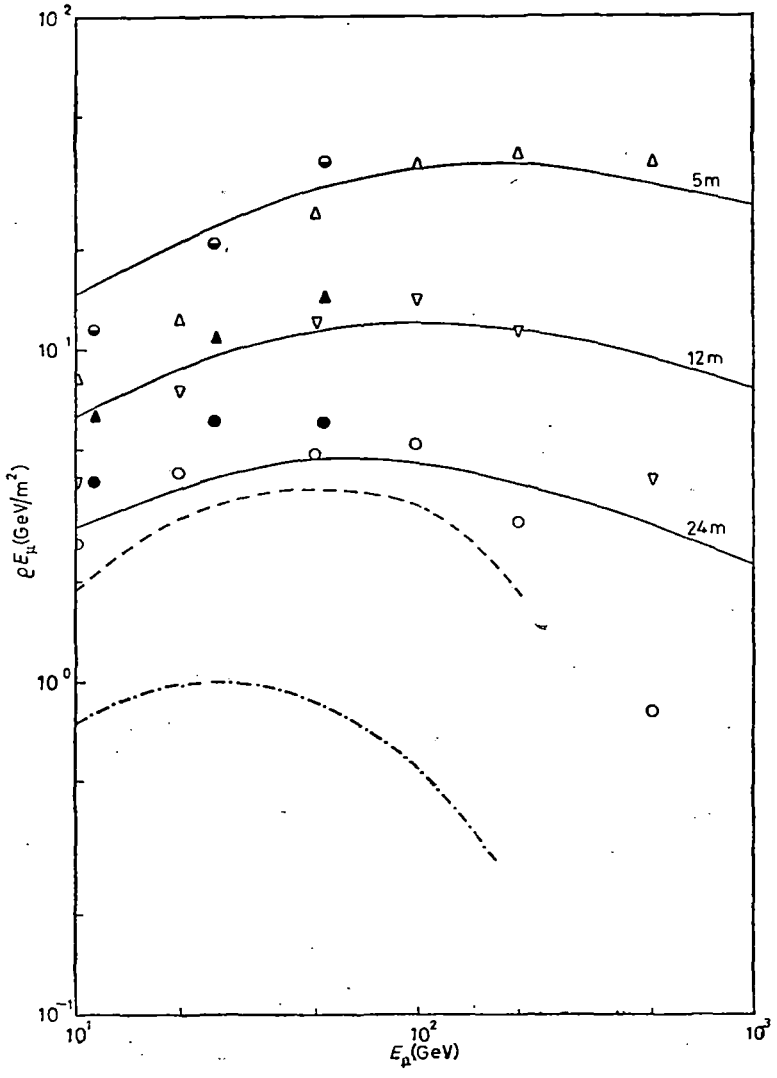

Fig. 6

8540 BASAK

AUTHOR PLEASE NUMBER FIGURES

Fig. 7

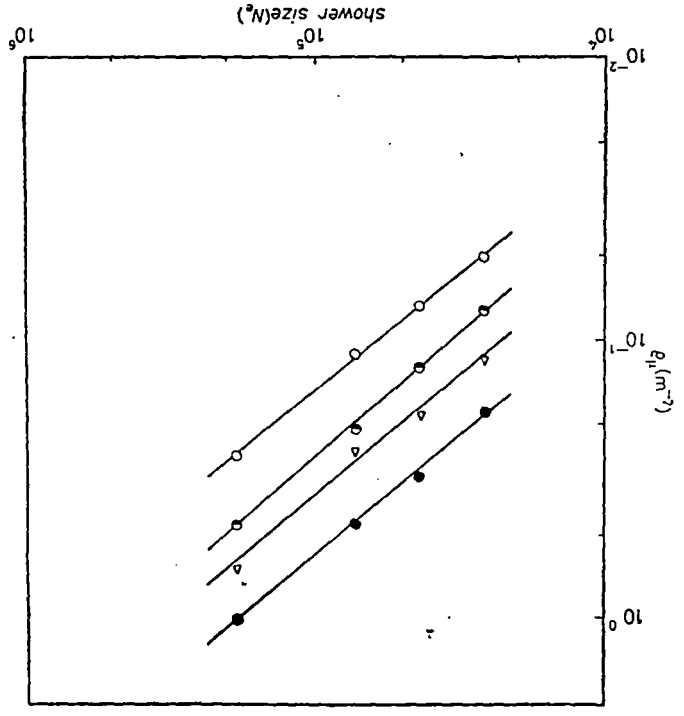

...clear Instruments and Methods in Physics Research 227 (1984) 167–172
...rth-Holland, Amsterdam

A NEW MULTIDETECTOR SYSTEM WITH MAGNETIC SPECTROGRAPH FOR STUDY OF COSMIC RAY EXTENSIVE AIR SHOWER COMPONENTS

D.K. BASAK, N. CHAKRABARTY, B. GHOSH, G.C. GOSWAMI, N. CHAUDHURI, N. MUKHERJEE, M. GOSH and S.K. SARKAR

Department of Physics, University of North Bengal, Darjeeling, India

Received 29 November 1982 and in revised form 9 January 1984

An array of detectors for simultaneous observation of different components of cosmic ray extensive air showers (EAS) is described. The detector array, comprising plastic scintillation counters as electron detectors, magnetic spectrograph units and a muon flash tube chamber as muon detectors and a large volume multiplate cloud chamber as hadron detector has been set up and is now being operated at NBU campus. The array of detectors is sensitive to air showers initiated by cosmic primaries of energy in the range 10^{14}–10^{15} eV.

1. Introduction

Nuclear multidetector systems continue to be of importance in ground based observatories engaged in high energy gamma ray astronomy and primary cosmic ray investigations. Very high energy primary gamma rays, protons or heavier nuclei have very low fluxes and consequently satellite studies are not feasible. The present status of observations using ground based techniques indicates a need for new and improved observatories at new sites. This paper describes a new ground based multidetector system that has been established for use in the search for high energy gamma rays and primary cosmic rays that develop into extensive showers of particles in the atmosphere.

2. Experimental arrangement

2.1. The air shower array

The relative position of each of the particle detectors is shown in fig. 1. The layout of the array is based on the arrangement of detectors in a sqaure symmetry. The electron density detectors are scintillation counters constructed with BARC * plastic scintillators of two different sizes: 0.25 m^2 and 0.125 m^2. These detectors are arranged at various locations covering an area 600 m^2 in such a way that small-area detectors are near the centre of the array. The array set up on the ground level is located near a 10 m high magnetic spectrograph housing. This magnetic spectrograph housing limits the zenith angular acceptance of the incident showers to a few degrees.

The array set up also includes a cloud chamber (not shown in fig. 1) of size 1 m × 1 m × 0.8 m with 13 lead plates inside (thickness 1 cm each) as hadron detector and three GM counter trays (not shown in fig. 1) and one neon flash-tube chamber as muon detectors. A three-fold coincidence of any three adjacent detectors near the array centre produces a master pulse which triggers the data handling systems, high voltage flash tube units in the spectrographs and flash chamber muon detector and cloud chamber control unit.

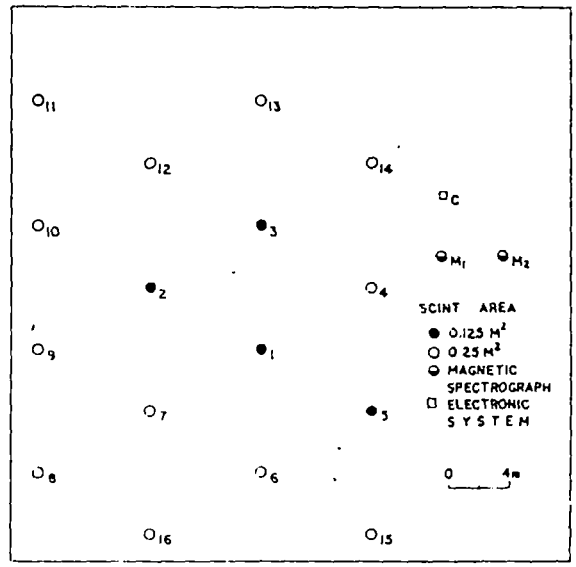

Fig. 1. Schematic diagram of air shower array.

* BARC, Bhabha Atomic Research Centre, Bombay, India.

2.2. Magnetic spectrograph units

Two magnetic spectrograph units at a separation of 4 m have been established in a housing which is located at a distance of 15 m from the array centre. Each unit is constructed using a rectangular solid iron magnetic block. These solid iron blocks were constructed [1] using low carbon content steel plates 12.5 mm thick. The plates are of size 180 cm × 125 cm with a rectangular hole of 19 cm × 35 cm at the centre. The thickness of the solid block thus formed by installing the iron plates one after another is 105 cm. The power requirement when wound with 600 turns of appropriate copper wire on the longer arms of the block and operated at 15 A current is 2.3 kW. Both longer arms of the magnet wound with wires have been used in the present investigation for deflection of EAS muons by using four accurately aligned muon flash-tube trays, two above an arm and two below, to locate the trajectory of the incident particle before and after passing through the solid iron magnet. The arrangement of the magnetic spectrograph is shown in fig. 2. An absorber of concrete and brick ~ 1 m thick on the roof about 1 m above the spectrograph units is provided to remove electronic components. Additional lead absorbers could be placed above the top tray of the spectrograph for this purpose. The information of the muon triggered neon flash-tube glows for the location of particle trajectories are obtained in digitised form. Each tray consists of eight layers of tubes which are staggered in such a way that a single particle passing through an array must traverse at least four trays (FT_1, FT_2, FT_3, FT_4). The tubes in each tray are placed in slots milled accurately in 'duraluminium' bars by means of a milling machine at CMRI **. The horizontal separation of the tube centres is 1.999 ± 0.002 cm which is referred to as one tube separation (t.s.). The vertical separation between the tube centres in a pair of adjacent layers is 2.8 cm. The flash tubes are 1.5 cm in diameter containing neon at a pressure of 60 cm Hg. A high voltage pulse of about 4.5 kV/cm with a rise time 0.75 μs is applied to the thin aluminium electrodes placed between layers of the tubes. 5 μs after the passage of a muon through the spectrograph by a trigger generated by the 3-fold coincidence of the scintillation counters (D_1, D_2, D_3). The tube discharges after the passage of the muon are recorded digitally and are printed on paper tape by means of a line printer. From the recorded coordinates of the passing muon at the four levels of detection in the spectrograph, its deflection in the magnetic field is calculated. The momentum of the muon is determined from the relation:

** CMRI: Central Mechanical Research Institute, Durgapur, India.

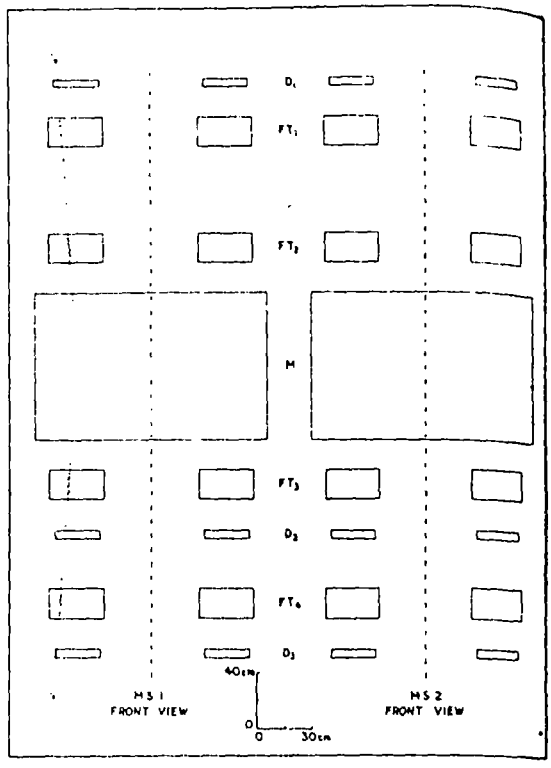

Fig. 2. Schematic diagram of magnetic spectrograph units.

$$P = 21.96/\Delta \text{ GeV}/c,$$

where Δ is the deflection in t.s. units and the constant in the numerator is the product of the geometrical factor of the spectrograph and the line integral of the magnetic induction. The maximum detectable momentum is given by

$$P_{\max} = \frac{21.96}{0.4266\sigma_t} \text{ GeV}/c.$$

Its value is 440 GeV/c for $\sigma_t = 0.117$ t.s., the probable error in track location. The lowest momentum that can be measured with the spectrograph is 2 GeV/c.

2.3. Electron density detectors

The scintillators used in the detectors are of two different sizes: 0.5 m × 0.25 m and 0.5 m × 0.5 m with the same thickness of 5 cm. A Dumont 6364 photomultiplier tube mounted suitably to view the scintillator forms the detector. The pulses from all the 16 detectors are amplified by preamplifiers with a gain of ≈ 20 each and are then sent to the main laboratory where they are again amplified by main amplifiers of appropriate gain. The main amplifier output saturates at 10 V, but the advantage of this amplifier is that it preserves the original shape after amplification except beyond the satura-

tion region. In the next stage, this pulse is fed to the 'Sample and Hold' circuit [2] which keeps the pulse stored for about ~ 3 μs by charging a condensor. At the end of ~ 3 μs, this condenser discharges and is ready to accept information for the next event. Up to this stage, all pulses from the detectors are accepted. The performance of each detector was studied while in calibration by measuring its single particle pulse height. The variation of pulse height from the centre of the detector to its edge was within ± 10%. The differential pulse height spectrum for vertical muons has a standard deviation of 40%.

2.4. Flash-tube chamber: muon detector

This consists of 9 layers of neon flash tubes installed in a chamber with a cover of 5 cm lead to get rid of electrons. Each layer contains 54 tubes arranged in such a way that a single particle passing through the flash chamber must discharge the tubes lying on its trajectory. The flash-tube chamber covers an area 1 m × 1 m for the location of the muon trajectories. The trigger pulse generated from the Master Control Unit (MCU) (fig. 3) is fed to the grid of a thyratron. The output pulse from the thyratron fires a second thyratron which in turn discharges a condenser (0.5 μF) charged to + 12 kV through a 100 Ω noninductive resistor. The resulting high voltage pulse is applied to the electrode plates between the layers of the flash tubes. The master pulse

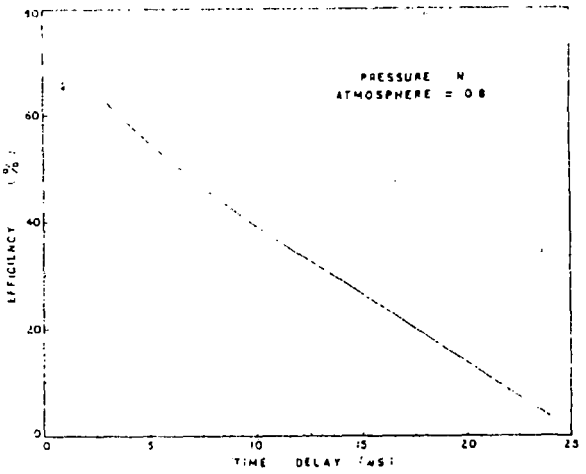

Fig. 4. Internal efficiency of the neon flash tubes as a function of delay time.

from the 3-fold coincidence of the particle density detectors operates a relay for winding the film in the camera which records the glow information of the event photographically and also for paralysing the first thyratron for a certain interval of time. The internal efficiency of the neon flash tubes in the flash tube chamber is shown in fig. 4 as a function of delay time between the passage of the muon through the chamber and the air shower trigger pulse. An example of a flash

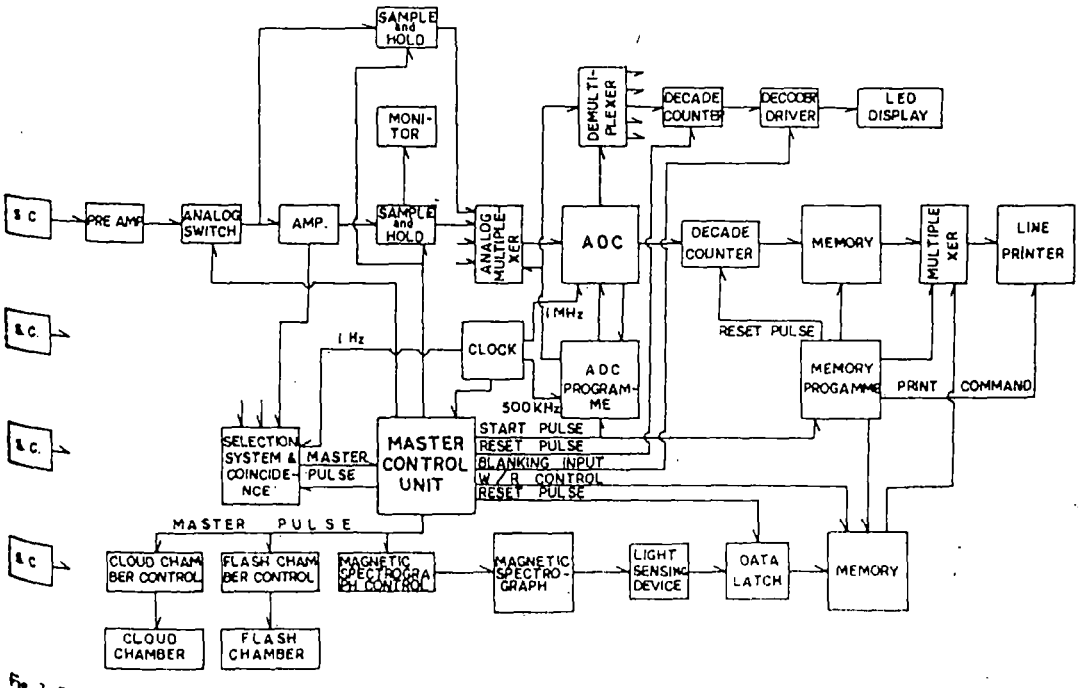

Fig. 3 Block diagram of electronic systems.

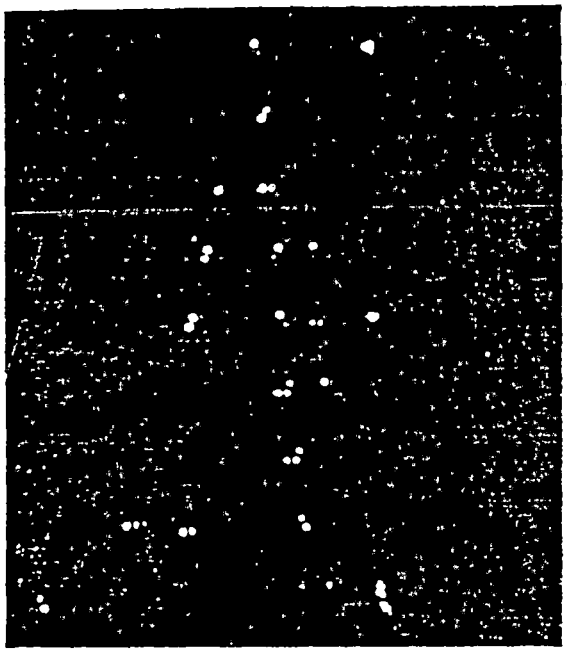

Fig. 5. An example of a muon track in the neon flash-tube chamber.

chamber record at the minimum delay time is shown in fig. 5

3. Data acquisition, storage and transfer

Fig. 3 shows the diagram of the system for data handling in the NBU air shower experiment. The analog outputs from all the 16 detectors of the array after amplification first by preamplifiers and then by main amplifiers are fed to the 'Sample and Hold' circuits by charging capacitors for about ~ 3 μs after the triggering of the MCU by a master pulse generated from a 3 fold coincidence of any three of the adjacent particle density detectors in the array (detectors 1–7). At the end of 3 μs, these capacitors will discharge and will be ready to accept the next input pulses. When the MCU is triggered, it in turn triggers the multiplexer unit, the analog-to-digital converter (ADC) [3], the ADC program unit and demultiplexer unit. They all will then be reset to zero. The multiplexer unit sequentially transfers analog data from all the 16 Sample and Hold units to the ADC for scanning the analog pulses one after another. The total time to scan all the channels is about 8 ms. The outputs from the ADC are demultiplexed by a demultiplexer whose outputs are connected to the display unit for visual display. The sequential outputs of the ADC are also connected to the memory unit for storing the digital information. After storage in the memory of all the information from the 16 detectors in the air shower array, these data are transferred to the printer for printing on paper tape. The adjustment is done in such a manner that a 10 V dc at the input of the ADC corresponds to a count of 1000.

The 3-fold coincidence master pulse also triggers the magnetic spectrograph control unit which then operates the spectrographs and the electrical information of the discharged neon flash tubes is fed, using suitable sensitive 'probes', to a separate memory unit. At the end of the printing of the air shower particle density information from the 16 detectors, the digital information of each of discharged neon flash tubes is transferred from the memory to the printer for printing on paper tape.

We have also the provision for independent operation of the spectrograph. Here the spectrograph control unit is triggered by the 3-fold coincidence of the scintillation counter trays placed vertically in each of the four arms of the spectrograph.

4. Operation and response of the array system

The master pulse generated from the coincidence of any three adjacent particle density sampling detectors triggers the MCU, cloud chamber control unit, magnetic spectrograph control unit and the flash-tube chamber control unit. As soon as the MCU is triggered it gives a 'Hold command' to the 'Sample and Hold' circuits, switches off the input lines by an analog switch and disconnects the coincidence circuit from the MCU and sends a start pulse to the ADC program unit.

Normally, the preset counters in the ADC program, the analog multiplexer, demultiplexer addresses are reset to zero and the ADC will not scan any input voltage fed at its input. Once the ADC program unit is triggered, it connects all the pulses at the output of the 'Sample and Hold' circuits by an analog multiplexer one after another to the ADC. The analog pulse at the input of the converter will then charge a condenser of capacitance 0.1 μF by means of a constant current source (linear ramp generator) to a voltage equal to the input pulse amplitude to be measured. The charging time of the condenser to a voltage equal to the input voltage is measured by means of a 1 MHz clock pulse. When the ADC scan for the first channel is over, the memory program unit controlling the ADC gives a 'write' pulse to the memory for writing the digital information in the memory. As soon as the counting in the first channel is over, the ADC program initiates the multiplexer to connect the second channel to the ADC for scanning and then writing in the memory. In this way, it allows the connection of all the 16 channels one after another to the ADC for scanning and writing in the memory. For a visual check the digital outputs from the ADC for each channel are demultiplexed and dis-

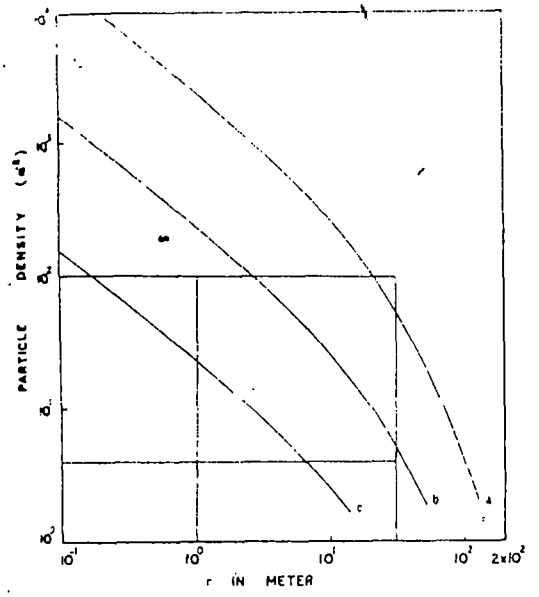

Fig. 6. Present response capability of the array. Shower size: curve (a) 10^6, curve (b) 10^5, curve (c) 10^4

played by seven-segment LEDs. At the end of a 'write' pulse, a 'read' pulse is derived from the memory program unit which is then operating on the memory unit for recording the digital information on paper tape by a line printer.

One end of each neon flash tube is attached to a probe. The function of the probe is to convert the tube discharge information into electrical pulses. The electrical pulses carry the information about those neon flash

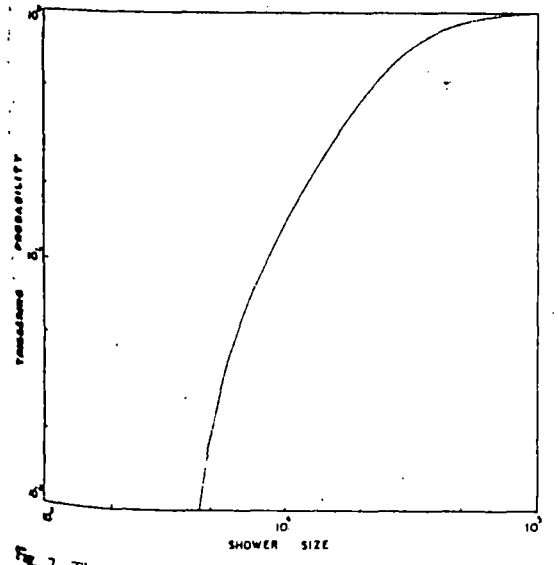

Fig. 7. The average triggering probability for the array of detectors as a function of shower size. $s = 1.25$.

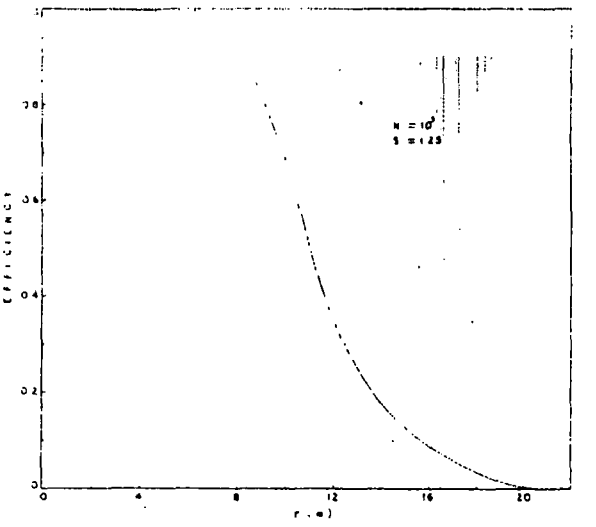

Fig. 8. The efficiency of detection of the array as a function of distance from the centre of the array.

tubes which are flashed due to passage of a muon through the flash tube trays. At the end of recording the information from the 16 density detectors and the discharged neon flash tubes, the analog switch is opened and it switches on the input lines for the next cycle.

The response capability of the array is shown in fig. 6 as the area bounded by four lines. Two horizontal lines show the dynamic range and the two vertical lines indicate the range of distance for density sampling. The present operation is being done by a trigger based on 3-fold coincidence under the threshold condition of one particle per detector. The average triggering probability for the array of detectors has been calculated as a function of shower size and s, using the Poissonian density distribution. The results for $s = 1.25$ and the triggering conditions on detectors within 8 m from the centre of the array are shown in fig. 7. The efficiency of detection as a function of distance from the centre of the array is shown in fig. 8. This has been calculated on the basis of NKG function densities at the individual detectors, each superposed with a Gaussian error term. The fluctuating densities for each shower size and s are used to discover whether the shower satisfies the triggering conditions for its selection.

5. Conclusion

The array of detectors described is capable of recording simultaneously information about electrons, muons and hadrons in air showers arriving near sea level. The momentum spectrum of air shower muons in the range 2-440 GeV/c will be studied by two magnetic spectrograph units. The shape of the energy spectrum of muons

depends on the primary composition. If a correct model for high energy nuclear interaction is used for the calculation, a comparison of the measured muon spectra and the calculated spectra for different primary nuclei will enable a study of the mass composition of primary cosmic rays.

The Department of Atomic Energy, Government of India, is thanked for granting financial assistance for the construction of the apparatus and continuance of the work. The Department of Education, Government of West Bengal, has provided some financial assistance for this project.

References

[1] B.C. Nandi and M.S. Sinha, Acta Phys. Hung. 29, suppl. 1 (1970) 529.

[2] G.C. Goswami, B. Ghosh, M.R. Ghoshdastidar and N. Chaudhuri, Nucl. Instr. and Meth. 199 (1982) 505.

[3] G.C. Goswami, B. Ghosh, M.R. Ghoshdastidar, S.K. Sengupta and N. Chaudhuri, Nucl. Instr. and Meth. 197 (1982) 375.

Neon Flash Tubes as Charged Particle Detectors

N. Mukherjee, S. Sarkar, D.K. Basak and N. Chaudhuri

University of North Bengal
Darjeeling 734 430

Special type of neon flash tubes have been used for recording the trajectories of high energy charged particles. The technique has been developed and the detector system constructed has been applied to cosmic ray physics experiments. A brief account of the neon flash tube technique as developed at the North Bengal University Centre is presented.

Introduction

Localization of the trajectory of a high energy charged particle can be done among other methods by arrays of long neon flash tubes. The advantage of the technique is that a larger collection area for detecting high energy charged particles can be obtained. The glass tubes are made 1-2 m long and 1-2 cm diameter, and are filled with 98% Ne, 2% He. One end of the tube has a flat end window for observing the flash discharge. This technique has been developed at North Bengal University and applied to experiments in Cosmic Ray Physics Laboratory.

The principle of operation

An electric field is applied across the flash tube for a few microseconds after the passage of a particle through it. The primary and the subsequent secondary ionisations cause an electron avalanche in the tube which in the presence of applied high voltage pulse initiates a glow discharge in the tube. This discharge giving a flash occurs in those tubes in an array through which the particle has passed. Other tubes in the array do not flash.

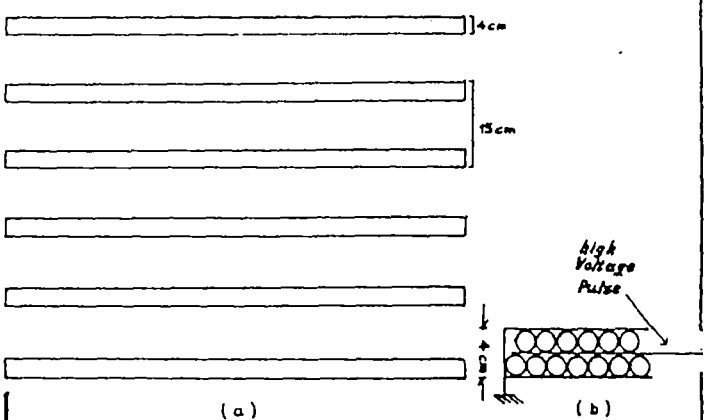

Fig. 1: The neon flash tube chamber.

THE AUTHORS

Shri N. Mukherjee, Lecturer in Physics in one of the colleges of the University, has been involved in the development of neon flash tubes as charged particle detectors.

Shri S. Sarkar of the Cosmic Ray Laboratory of the University has contributed to the development of electronics for the neon flash tube detectors.

Dr. D.K. Basak has contributed to the development of digital electronic system for triggering the neon flash tube arrays by a high energy charged particle.

Dr. N. Chaudhuri is the Head of the University Science Instrumentation Centre at the University of North Bengal.

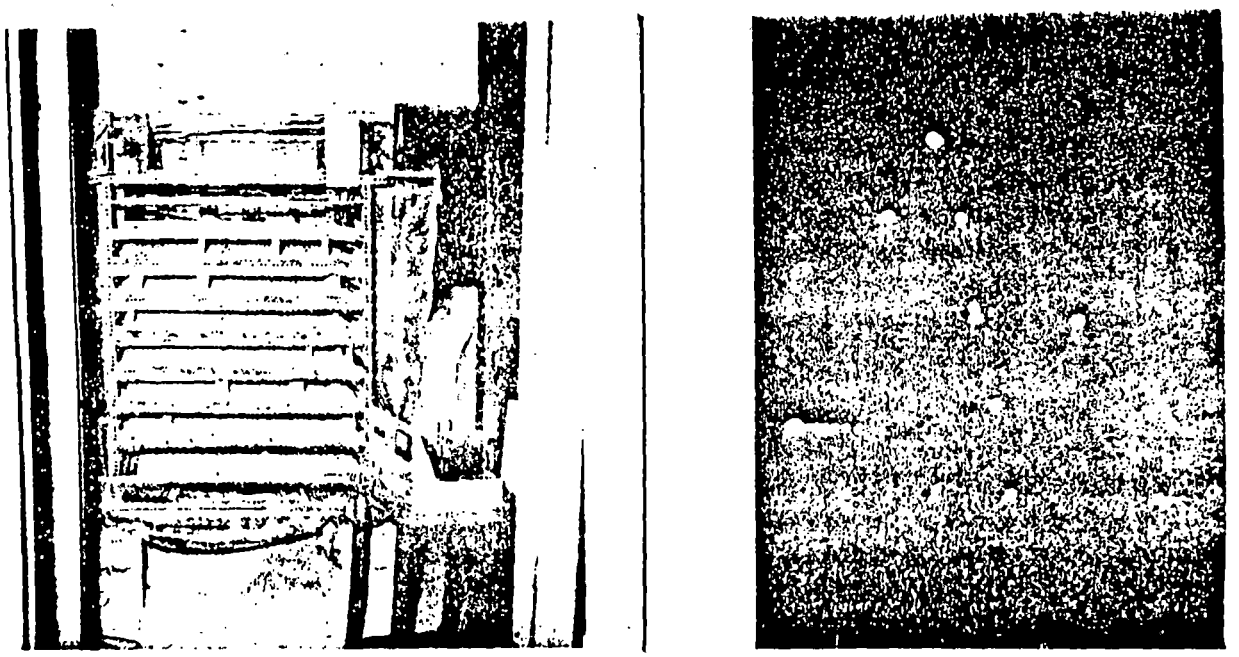

Fig. 2: A photograph of neon flash tube chamber along with a charged particle trajectory.

The neon flash tube chamber

The neon flash tube chamber constructed at this Centre is shown in Figure 1. It consists of six layers of neon flash tubes installed in a chamber with a cover of 5 cm of lead to get rid of electrons. Each layer contains 54 tubes arranged in such a way that a single particle passing through the flash chamber must discharge the tubes lying on the trajectory of the particle. The neon flash tube chamber covers an area of 1m x 1m for the localisation of muon-trajectories.

A photograph of the neon flash tube chamber along with a charged particle trajectory is shown in Figure 2. The arrangement of the flash tube arrays in the magnetic spectrographs at the North Bengal University is projected in Figure 3. Figure 4 is an example of recorded cosmic ray particle trajectory.

External probe technique of recording particle trajectory

Instead of recording the neon tube flash by a camera, a technique has been developed e.g. D.K. Basak et al (Ref. 1) and Ayre and Thompson (Ref. 2) for observing electronically whether a neon flash tube has flashed. A small metal probe in the form of a thin disc at the end of a brass rod is placed close to the flat end of each flash tube (Figure 5.). When a tube gives a flash, a pulse of several volts is obtained across the resistor between the probe and the ground. This pulse differs distinctly from the high voltage noise pulse picked up by the probe from the high voltage pulse on the electrodes and also from the high frequency radiation from the discharge in the neon flash tube. This noise pulse has been reduced to a minimum by using proper shields and the pulse on the probe due to the flash in the tube has been used to trigger a multivibrator circuit which in turn operates a LED (Light Emitting Diode) display unit.

Operation of a single flash tube

A neon flash tube of internal diameter 1.5 cm

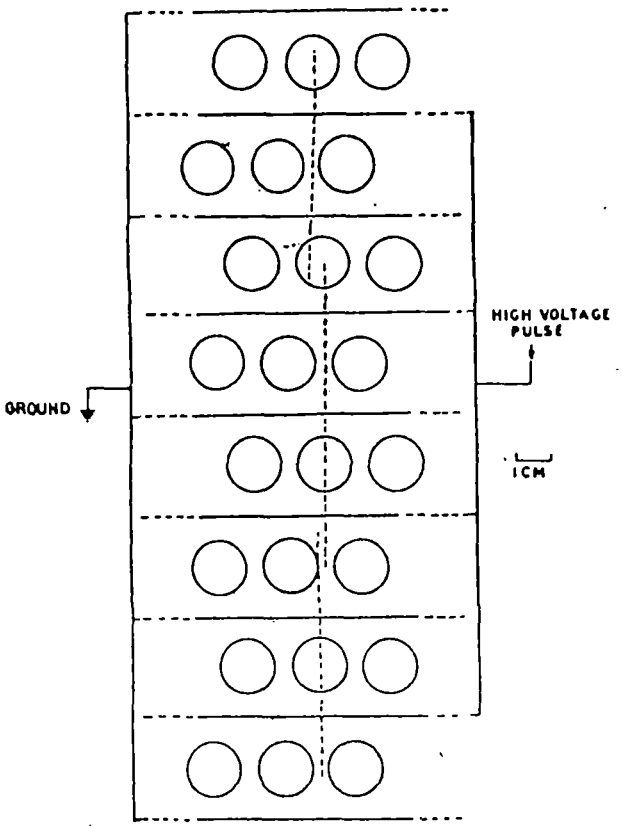

Fig. 3: The arrangement of the neon flash tubes in the magnetic spectrograph array.

filled at a pressure of 60 cm of Hg was placed between two aluminium electrodes. The entire tube together with the electrodes was enclosed in a metal cage of GI netting. Only the flat end window of the tube was kept outside the enclosure. The metal cage shielding was grounded at a single point which was found out by trial for a minimum noise pick-up. A thin brass disc of diameter 1 cm was placed very close to the flat end-window of the flash tube. The disc was connected to the ground through a resistor R (Figure 5). The voltage pulse across R due to discharge of the flash tube was fed to a multivibrator circuit through a capacitor C and the same circuit was used to control a LED display unit. For the reduction of the spurious glow of the LED display due to the high frequency electromagnetic radiation the entire electronic circuit together with resistor R and capacitor C is enclosed in another GI cage which was also grounded at a single point. The metal probe is connected to the resistor R by a shielded cable, the shield being attached to the second shielding cage. The glow of the LED display gives an indication of the discharge of the flash tube due to the passage of a charged particle through it.

Flash tubes in array

This method has been applied to each of the eight arrays of flash tubes, each containing 2m long 120 tubes (Figure 3). These have been used to construct two magnetic spectrographs (Figure 6) for the localisation of muon trajectories in cosmic ray air showers in an experiment running at the Campus of North Bengal University.

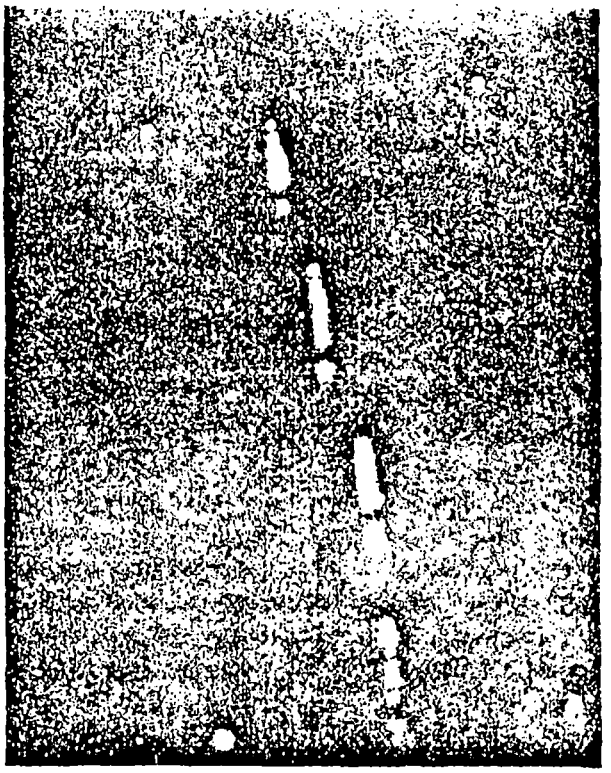

Fig. 4: An example of recorded cosmic ray particle trajectory.

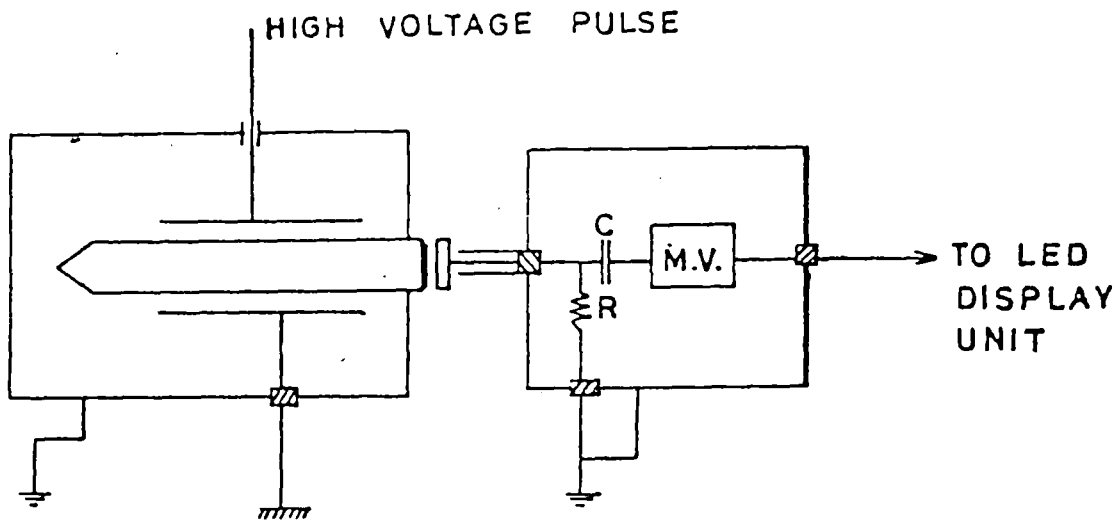

Fig. 5: Probe method of recording neon flash tube glow.

For recording the trajectory of the passing charged particle, the outputs of the multivibrator circuits are connected to an array of LEDs arranged on a board in the same order as that of the flash tubes in each of the arrays. The electronic circuit and LED display unit are shown in Figure 7. The trajectory of the charged particles passing through the flash tubes is thus displayed as the glows on the board of the corresponding LEDs. By using bi-stable multivibrator circuits, the glows of the LEDs are made stable for photographic recording of glow display for the determination of particle trajectory. The flash tube trays and the electronic circuits driving the display units were shielded separately by GI netting in such a way that the GI netting shields are perfectly insulated from all other neighbouring materials. The shielding cages are grounded at single points determined through a search for minimum noise pick-up. The high voltage 10 KV pulse of rise time 7.5 μs was used for the operation of the flash tubes and was applied across the flash tube electrodes 5 μs after the passage of a charged particle which triggers the high voltage pulser unit.

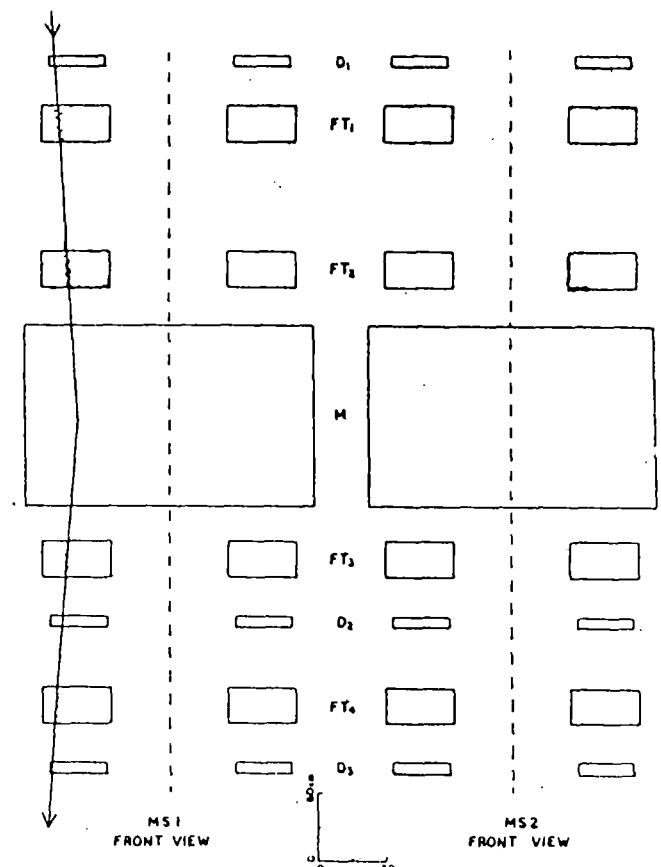

Fig. 6: The two muon magnetic spectrograph units.

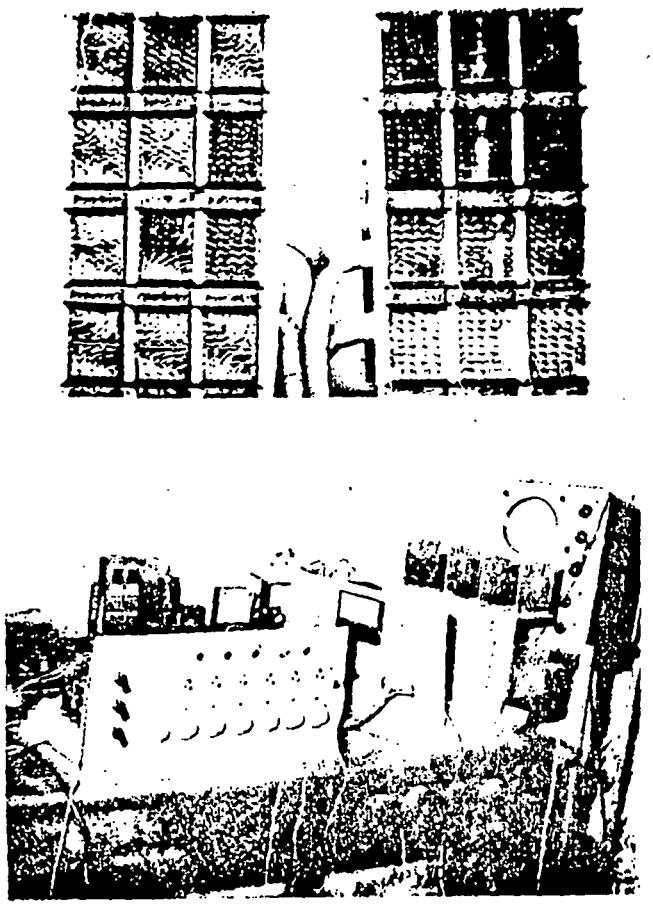

Fig. 7: The electronic circuit for triggering LED display unit.

Discussion

Perfect shielding and the grounding of the shielding cages at single points are the essential conditions for a noise free recording of charged particle trajectories through the array of neon flash tubes. It is very difficult to locate the optimum grounding points for the shielding cages. The slightest displacement from the optimum grounding points leads to an appreciable pick up of noise pulses.

References

1. Basak D.K., Chakravorty N., Ghosh B., Goswami G.C. and Chaudhuri N, Nucl. Inst. and Meth., 227 (1984) 167
2. Ayre C.A. and Thompson M.G., Nucl. Inst. and Meth., 69 (1969) 106.

North Bengal Univ. Review (Sci. & Techno.)
Vol. 5, (No. 1 & 2) 1984

COSMIC RAYS AT NORTH BENGAL UNIVERSITY
1. HIGH ENERGY PARTICLE INTERACTION PROCESSES.

N. Chakraborty, B. Ghosh, N. Mukherjee, D. K. Basak, S. K. Sarkar and N. Chaudhuri

Department of Physics, North Bengal University, West Bengal, India.

Received February 29, 1984 and Revised January 25, 1985

Abstract: A brief account of the development of cosmic ray research at NBU is presented here. Some representative results of the investigations are included to indicate the present state of research on electromagnetic particle interactions at ultra high energy.

1. *Introduction :* The cosmic ray research in India has a tradition over more than four decades now. The cosmic ray physics group at Calcutta which included among others Prof. D. M. Bose, Prof. Shyamadas Chatterjee, Prof. P. C. Bhattacharyya, Prof. R. L. Sengupta, Prof. M. S. Sinha, Prof. P. K. Senchaudhuri had close connections with other cosmic ray physicists in the country and outside, for example, Prof. H. J. Bhabha, Prof. L. Janossy, Prof. W. Heitler, Prof. B. Rossi, Prof. G. D. Rochester. The Calcutta group dispersed in the late sixties and formed several small groups and one of these came to N. B. U. soon after the University started in 1962.

Before coming to N.B.U. the members of the group had worked at high altitude station in Darjeeling on some aspects of secondary cosmic rays and also in underground stations at Maithon (West Bengal) on the properties of the penetrating components of the secondary cosmic rays. The various components of the secondary cosmic rays, indicated in Fig. 1, are the progeny of a flux of energetic particles from the pulsars, supernova and other very energetic celestial objects in the galaxies. The flux consists of protons, some heavier nuclei and some relativistic electrons. These particles spend millions of years wandering through the interstellar medium (ISM) before reaching our solar system. The relative intensities of these particles above energy of 4 GeV/nucleon are given in table 1.

In addition, there is a flux of ν_e (electron-neutrino) from various stars produced through β-decay ($p \rightarrow n + \beta + \nu_e$) processes. In the atmosphere when the primary protons and heavier nuclei undergo interactions with atmospheric nuclei a variety of new particles is produced. The nuclear interaction processes in the atmosphere are developed in cascades.

In the sixties at N. B. U., the excitement for research in cosmic rays was heightened due to the enthusiasm of the research workers of this new University. The group engaged their interest in the study of the secondary component consisting of the decay-products of pions (π) and kaons (K). In this paper a brief review is given of the cosmic ray research development at N. B. U. and some representative results of various studies made during the last fifteen years.

2. *Study of muons with visual detectors :* In

the first five years (1965-70) of work a laboratory was set up with a large multiplate cloud chamber, scintillation detectors and G. M. counters. The multiplate cloud chamber mounted on a steel framework could be rotated and fixed at any zenith angle for the detection of very high energy muons for the study of their interactions with nuclei of iron and

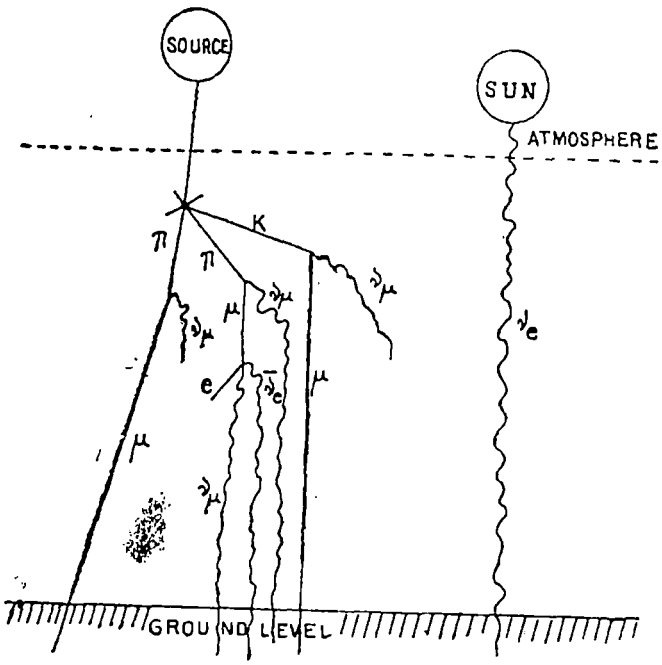

Fig. 1

aluminium placed inside it. The large area scintillation counters were built up for the selection of the high energy cosmic rays from any direction and for triggering the multiplate cloud chamber when the cosmic ray muon particles entered the chamber.

There are some advantages of using for such a study the cosmic ray muon (μ) beam from inclined directions. At the atmospheric depth 'X' the intensity of component of the cosmic ray beam at a zenith angle θ is assumed to be given by

$$J(X, \theta) = J_0 \exp(-X/L\cos\theta)$$

or $$J(X, \theta) = J_0 \exp(-d/L)$$

where $d (= X \sec\theta)$ is the oblique penetration path of particle of the component,

L is the mean attenuation-length of the component,

J_0 is the intensity at the production-level (i. e. X=0) of the component.

Now for the nuclear active component, $L = 128\ gcm^{-2}$ of air and this component is rapidly attenuated before arriving at sea-level from greatly inclined directions. The intensity of the electronic component generated from the materialisation process of the decay-photons of neutral pions is also dependent on exp ($-d/L$). For large d the electronic component arising from neutral pion and kaon decay is rapidly attenuated in air of radiation length $38\ gcm^{-2}$ for this component. The high energy muon-component arising through the decay of charged pions and kaons (branching ratio is $\frac{2}{3}$ can arrive at the ground-level because of its large radiation length in air. In the directions with large d the intensity of low-energy muons is reduced because of the increasing energy-loss and decay along large olique path whereas the intensity of high-energy muons is increased because of the increased decay-probability of the parent mesons.

2.1. *Directional intensities of muons at 16°N Geomagnetic latitude :* The basic measurements at

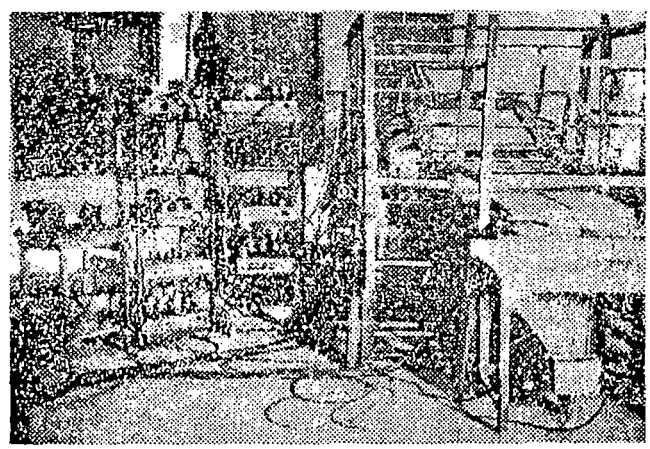

Fig. 2 (a)

our laboratory were performed with the help of a 'charged-practicle-telescope' that could point to different directions for detecting the muons above a

threshold minimum energy of 0.3 GeV. The actual duration of observations in various directions between the vertical and 90° to the vertical are given in table 2 with the values of the absolute intensities defined as the number of muons detected per hour per m^2 within a solid angle of 1 steradian with the given zenith angular direction :

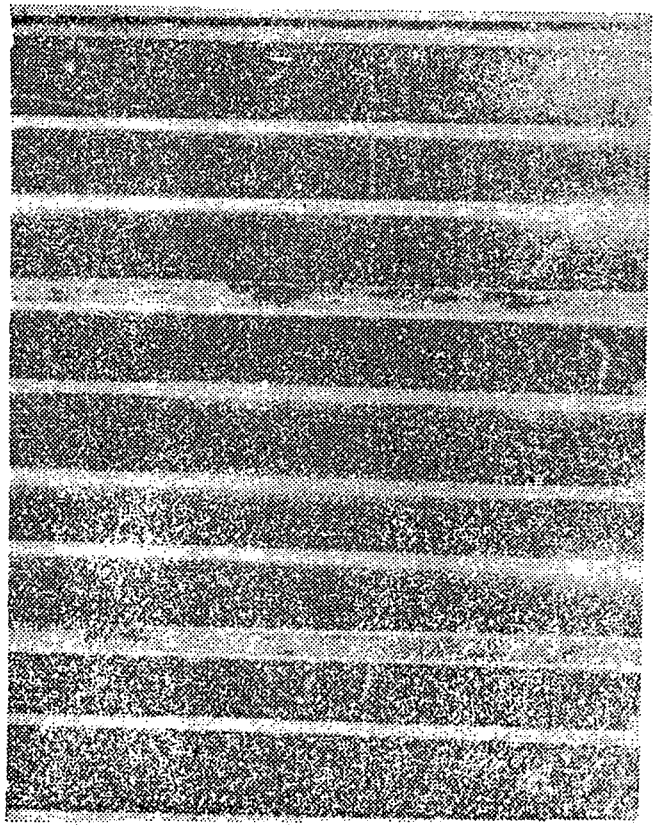

Fig. 2 (b)

2.2. *Muon interaction studies :* The characteristics of the muon interaction with nuclei of heavier atoms like iron (Fe), aluminium (Al) & lead (Pb) have been studied by visual observation in the cloud chamber containing layers of Fe, Pb and Al targets. This observation was carried out for about three years during the period 1972-75. Some representative examples of single muon detections and various other interaction phenomena are given in the following sub-sections. The properties of the muon as a 'heavy electron' are :

rest mass of the muon = 206 m_e [m_e – mass of the electron
$= 9.1 \times 10^{-28}$ gm]

electric charge of the muon = e [charge of the electron
$= 1.6 \times 10^{-19}$ coulomb]

Intrinsic spin of the muon = $\frac{1}{2}$

magnetic moment of the muon = (1.001162 ± 0.000005) $e/2m_u$

2.2.1 *The occurence of single muons :* An example of a single muon arriving from the zenith angular direction of 70°-80° and entering the multiplate cloud chamber (fig. 2a) is shown in fig. 2 (b). Total number of such photogrphs obtained during the period of observation in three zenith-angular directions is 20,000.

2.2.2 *Nuclear interactions of muons :* The main interest in muon studies has been in the study of characteristics of nuclear interactions of muons. A number of cases of nuclear interactions of muons

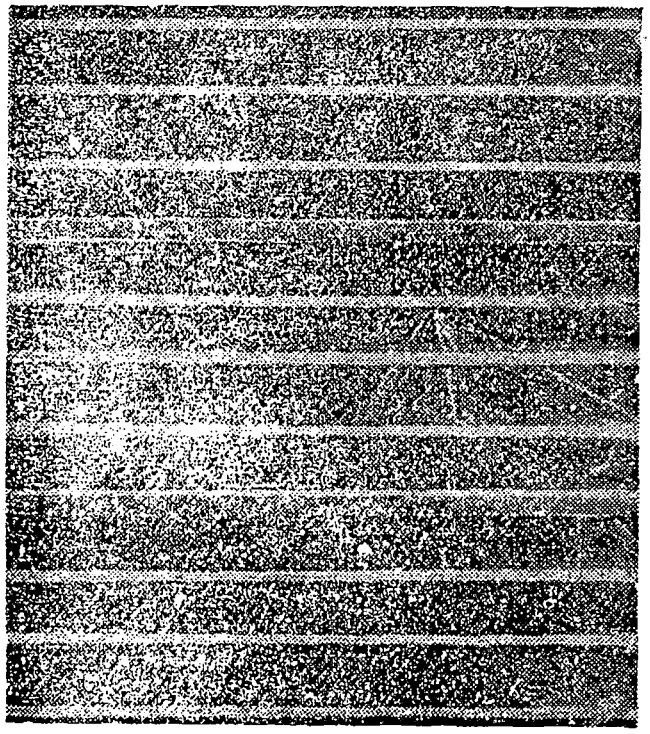

Fig. 3

were observed in the cloud chamber. One example is shown in fig. 3 which depicts that the single muon in collision with nuclei in target material produces a

variety of particles. More than eight thinly ionising secondary particles, mostly pions, penetrated more than 2 radiation lengths of lead without subcascade multiplication. This chracteristic and production of

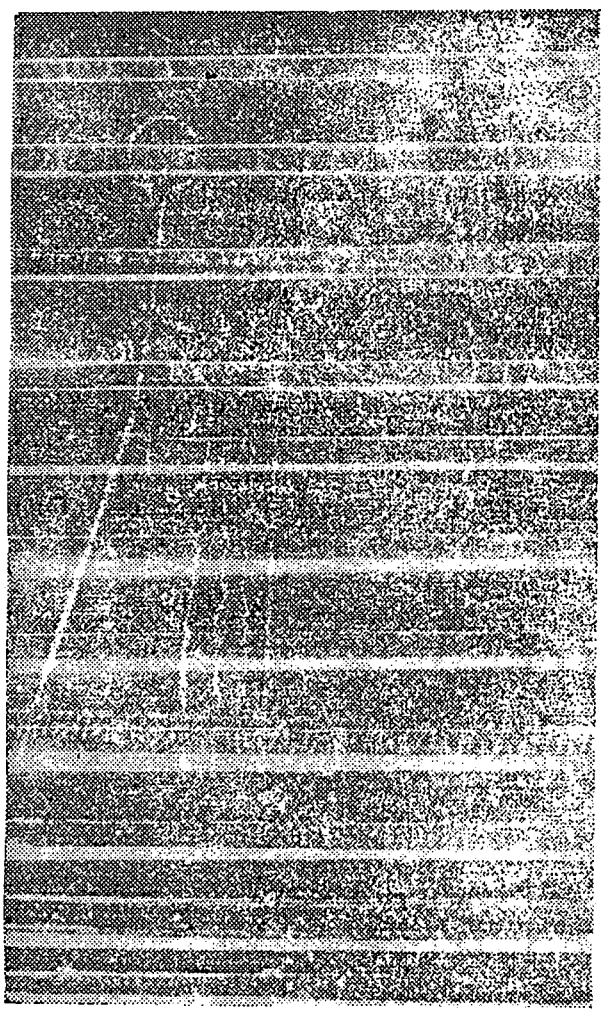

Fig. 4

a few heavily ionizing particles are the features of a nuclear interaction. The minimum energy transfer was estimated from the total track length in the multiplate chamber and the absorber below it. The primary muon energy was estimated from the total track length in various zenith angular directions. We have determined from direct observations the probability of nuclear interactions of muons and some representative results are given in figure 10. In this figure the average nuclear interaction cross sections of muons have been plotted against the estimated energy transfer. Figures (a) and (b) indicate the cross sections for iron and lead respectively. The curve indicates the theoretical cross-section values according to the 'vector meson dominance' (v m d) model for K=1, K being the energy transfer in photon-nuclear interaction. The circles with the error-marks indicate our experimental values.

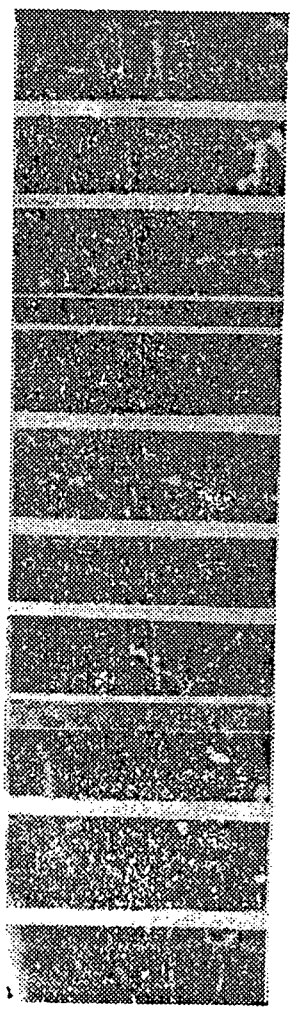

Fig. 5

2.2.3 *Direct production of electron-pairs by Muons* : We have observed muon-interactions in which the parent muons produced a pair of electron and positron in collisions with target of Fe and Al atoms. One example of 'direct pair production' (dpp) event is shown in fig. 4. A tridant ($e^- - e^+$) pair

and the parent muon) appears in the bottom of the 4th producing plate. The low energy partner of the pair stops in the 5th iron plate while the high-energy one penetrates two more plates and then stops in the 8th plate. We have determined the probability of direct pair production of muons from visual observations of events in the cloud chamber. The dpp interaction cross-section has been evaluated and a sample of cross-section data is given in table 3.

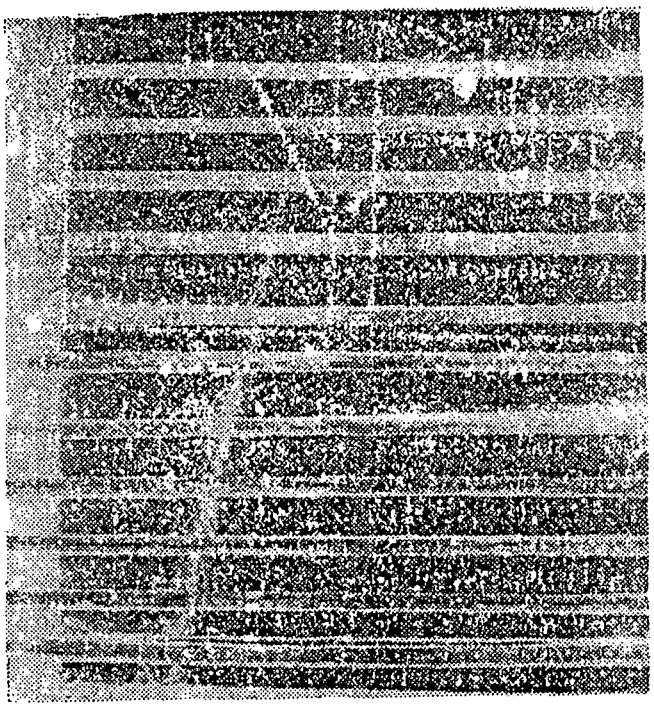

Fig. 6

QED : Quantam Electrodynamics

KP : Theoretical calculation of Kokoulin and Petrukhin [2]

MUT : Theoretical calculation of Murota, Ueda and Tanaka [1]

Bh : Theotetical calculation of Bhabha [3]

The experimental results given in the table—3 from the final analysis represent improvement over our earlier results [4]. Further this confirms the QED calculation of dpp process by Kokoulin & Petrukhin [2]. Other reported experiments which raised doubts on the validity of QED theory of dpp process in different regions of enengy transfer includes the works of Butt & King [5] and Jain et al [6].

2.2.4 *Muon-electron Knock-on Collisions*: In some cases high energy muons in the secondary cosmic rays knock out single electrons from the target atoms. An example is shown in fig. 5. The traversing muon knocks out an electron from an iron atom in the 4th plate and this high-energy knock-on electron stops at the 8th plate. This example demonstrates the behaviour of the muon as a 'heavy electron'.

2.2.5 *Muon bremsstrahlung*: The behaviour of the muon as a heavy electron was studied by

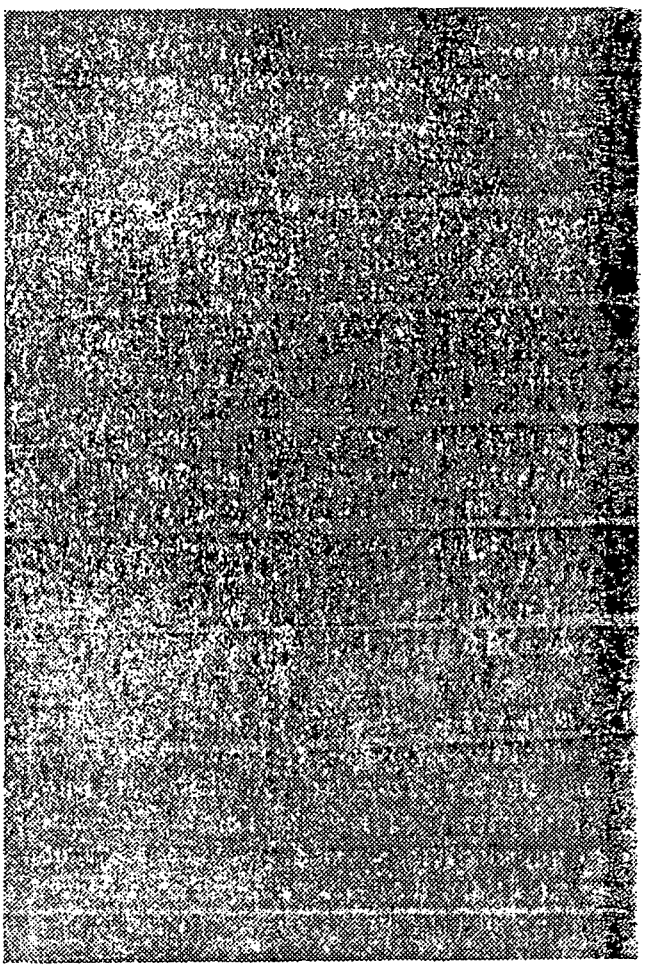

Fig. 7

observing the muon-induced electron cascade through bremsstrahlung production. An example of bremss-

trahlung shower by the muon is shown in fig. 6. The bremsstrahlung cross-section (at an underground depth of 148 mwe) in combination with very high energy dpp has been determined as a function of energy-transfer from cloud chamber observations. A sample of observed cross-sections is given in table 4.

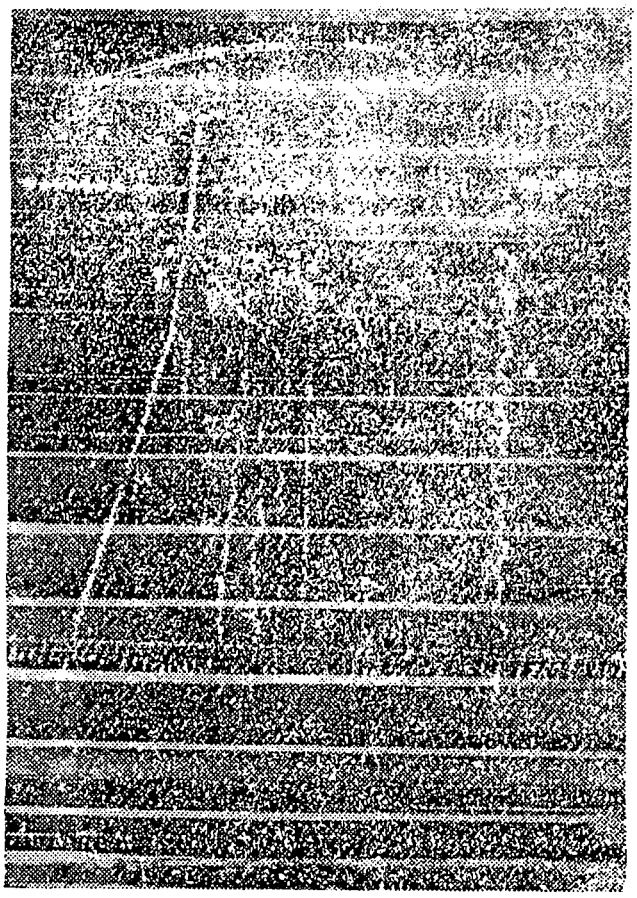

Fig. 8

2.2.6 *Horizontal bremsstrahlung shower in the atmosphere :* Events representing muon bremsstrahlung and muon-nuclear interactions of large energy transfer have been observed in the form of shower of electrons entering from air into the cloud chamber. The observed frequency of these interactions at an atmospheric penetration depth of 4×10^{3} gcm^{-2} is 46.8 m^{-2}Sr^{-1}hr^{-1}. An example of horizontal shower of electrons entering the cloud chamber from air is shown in fig. 7. As mentioned earlier the primary cosmic ray nuclei and the nuclear active component of cosmic ray nuclei are rapidly attenuated in large oblique path in greatly inclined directions. The detected air showers at the zenith angle 70°—80° are mainly due to ultra high-energy secondary muon bremsstrahlung and in very small part due to ultra high energy muon-nucleon interactions in the atmosphere. The photograph given may be an example of such atmospheric muon-bremsstrahlung event.

Fig. 9

2.2.7 *Parallel multiple muons :* Interesting phenomena of parallel multiple muons from vertical and inclined directions have been detected in the cloud chamber. These events are interpreted as the decay-products of pions produced in muon-nuclear and muon-bremsstrahlung interactions. An example of parallel multiple muon event is shown in fig. 8.

2.2.8 *Muon decay tracks*: In the series of observation with multiplate cloud chamber several examples of muon decay tracks have been detected. An example is given in fig. 9. It shows a muon entering the multiplate cloud chamber traverses several plates and then it slows down (showing a thick

track) and eventually stops in the 9th plate and decays. The associated decay electron proceeds in the upward direction and stops in the 7th plate.

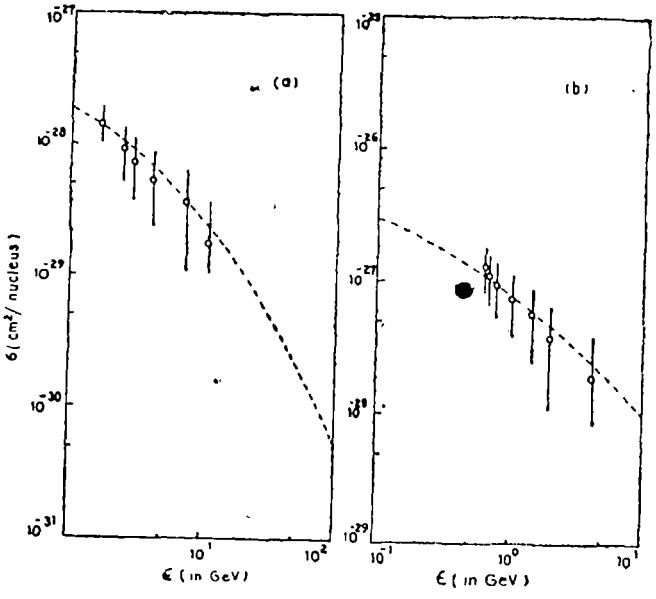

Fig. 10

3. *Conclusion* : The cosmic-ray muon has been used as the 'heavy electron' to study its interaction behaviour with matter within the theoretical frame of quantum electrodynamics (QED). The conclusion obtained from the N. B. U. cosmic ray investigations is the following : the fundamental concepts of QED have been found to be compatable electromagnetic interactions involving energy-transfer upto 100 GeV that has been directly observed.

4. *Current projects* : The Department of Atomic Energy (DAE), Govt. of India sanctioned a new project in 1978 to the cosmic ray group at North Bengal University for an investigation of hadrons and muons in cosmic ray extensive air shower. An array of scintillation detectors has been constructed to record the air showers initiated by primary cosmic ray particles in the energy range $10^{14}-10^{16}$ eV in the atmosphere. The detecting array covering an area of 600 sq. metre is situated in the N. B. U. campus near the Department of Physics. Two magnetic spectrographs, each weighing 16 tons have set up near the array to detect the air shower muons and to measure their momenta, signs of associated electric charge. These measurements, taken in concidence with the measurements of the electron densities by the scintillation detectors of the air shower array can yield information on the high-energy nuclear interactions responsible for the development of an air shower and on the nature of the cosmic ray particles.

A new feature to time precisely by each of the several fast detectors the arrival of the shower front at the individual detector included in the array will be added in another project which is now under consideration of DAE. The array of the detectors with this feature of accurate timing will enable a search for narrow-angle anisotropy in the shower arrival directions. Such measurements taken in conjunction with the measurements on air shower muons will enable to draw conclusions on localised sources of ultra high energy cosmic gamma rays.

Table—1

Relative intensities of the primary cosmic rays

Protons (z=1)	α-particle (z=2)	Light Nuclei (z=3−5)	Medium Nuclei (z=6−9)	Heavy Nuclei (z≥10)	Very Heavy (z≥26)	Relativistic electrons
100	5.00±0.2	0.09±0.03	0.33±0.02	0.11±0.02	0.03±0.01	1% of protons

Table—2

Absolute intensities of cosmic ray muons

Direction of observation	Actual time of observation (min)	Minimum energy (GeV)	Absolute Intensity ($m^{-2}hr^{-1}sr^{-1}$)
Vertical	4695	0.3	323640±1800
45° to the vertical	15190	0.3	150120±954
75° ,,	6790	0.3	12562.4±327.6
85° ,,	6570	0.3	2538±176.4
90° ,,	7495	0.3	442.8±28.8

Table—3

DPP cross-section in Al target of thickness 0.405 g cm^{-2} at various zenith angles.

Mean Zenigh angle	Energy transfer interval (MeV)	Experimental cross-section (cm^2/g)	Predictions of QED (cm^2/g) KP	Bh	MUT
0°	3-30	(6.6±2.1)×10^{-5}	5.72×10^{-5}	5.5×10^{-5}	8.16×10^{-5}
45°	3-30	(8.2±2.5)×10^{-5}	7.71×10^{-5}	7.6×10^{-5}	1.02×10^{-4}
75°	3-30	(1.5±0.4)×10^{-4}	1.45×10^{-4}	1.4×10^{-4}	1.71×10^{-4}

Table—4

Bremsstrahlung Cross-section in combination with very high energy dpp production in lead (Pb) target of thickness 70.9 g/cm^2 in different energy transfer intervals :

Energy transfer (GeV)	Observed No. of showers	Experimental cross-section (cm^2/g MeV)	Theoretical (QED) KP	Cross-sections cm^2/gMeV MUT
1-2	44	(4.0±0.6)×10^{-8}	4.21×10^{-8}	4.89×10^{-8}
2-3	16	(1.4±0.4)×10^{-8}	1.39×10^{-8}	1.53×10^{-8}
3-4	7	(6.3±1.4)×10^{-9}	6.21×10^{-9}	7.03×10^{-9}
4-6	6	(2.7±1.1)×10^{-9}	2.75×10^{-9}	3.02×10^{-9}
6-8	3	(1.5±0.8)×10^{-9}	1.29×10^{-9}	1.42×10^{-9}
8-12	3	(6.8±3.9)×10^{-10}	6.0?×10^{-10}	6.55×10^{-10}

Acknowledgement : The initial work was made possible by the loan from DAE, Govt. of India of two cloud chambers constructed in earlier projects at Bose Institute, Calcutta. In 1979 two solid iron magnets were transferred by an order of DAE from R. E. College, Durgapur to NBU for use in the air shower project sponsored by DAE. The Govt. of West Bengal is thanked for some financial assistance. Prof. M. S. Sinha helped in the initial stage of constructing the magnetic spectrograph under the visiting faculty scheme of UGC.

REFERENCES

1. Murota T, Ueda A and Tanaka H, *Prag. Theoretical Physics*, 16, 482, 1956.
2. Kokoulin R. P and Petrukhin A. V. *Proc. 11th Int. Conf. on Cosmic Rays*, Budapest, 1970.
3. Bhabha H. J. *Proc. Roy, Soc.*, A 152, 559, 1935.
4. Chaudhuri N., Goswami B , *Nuovo Cimento*, A 65, 727, 1970.
5. Butt J. E., King D. T. *Phys. Rev. Lett.*, 31. 904, 1973.
6. Jain P. L., Kazuno M, Girard B, *Phys Rev. Lett.*, 32, 1460, 1974.
7. Berger and Seltzer, Nuclear *Science Series, Report No.* 39, NAS--NRC Sept. 15, 1967.

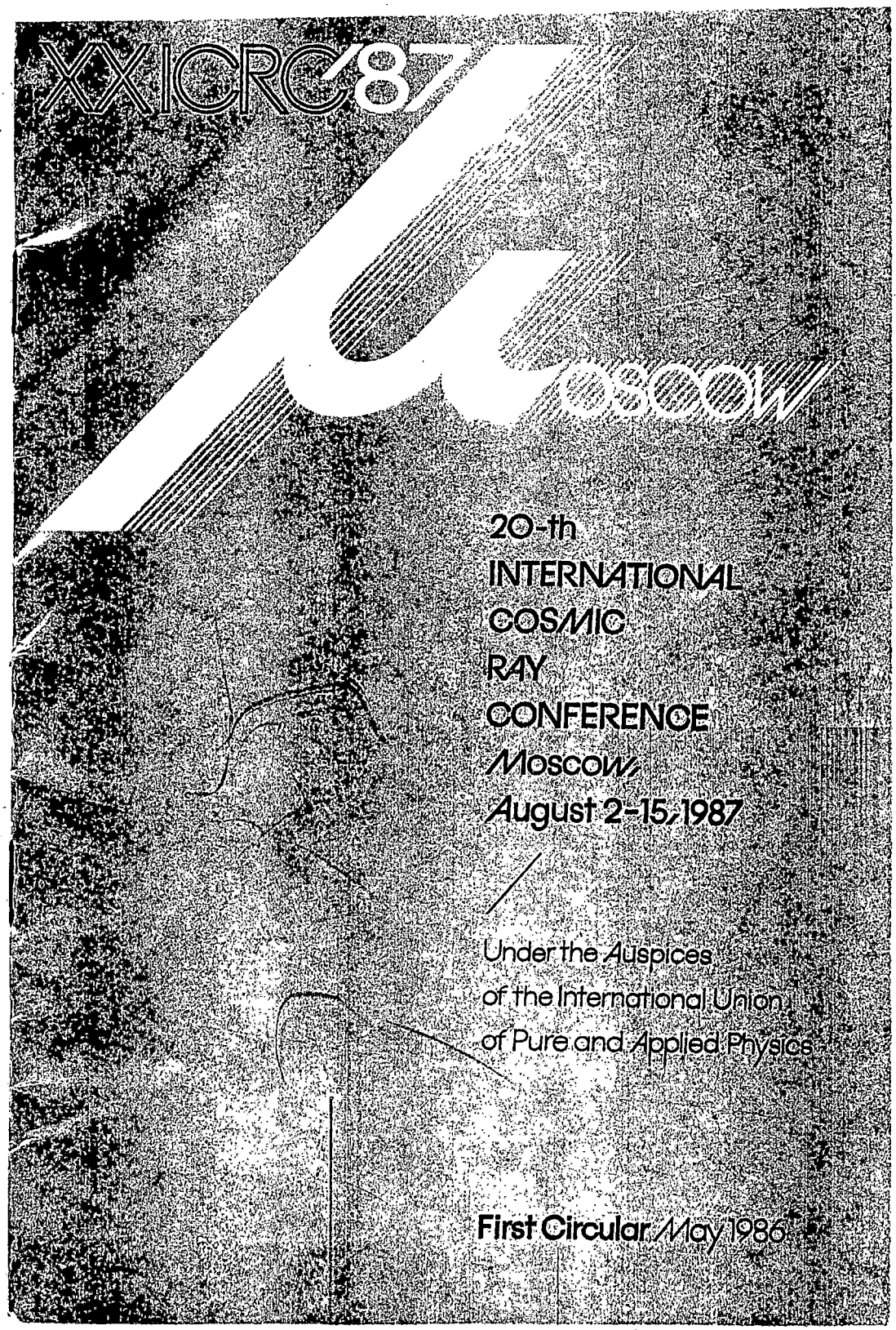

20-th INTERNATIONAL COSMIC RAY CONFERENCE

Moscow, August 2-15, 1987

Under the Auspices of the International Union of Pure and Applied Physics

First Circular / May 1986

NEW RESULTS ON ENERGY SPECTRUM OF MUONS IN EAS

Samir Kumar Sarkar, Narendra Nath Mukherjee, Mihir Kumar Roy, Mrinal Kanti Ghosh, Biswanath Ghosh, Dhiraj Kumar Basak and Nirmalendu Chaudhuri

High Energy Cosmic Ray Centre, University of North Bengal
North Bengal University(NBU), Dist.Darjeeling, India-734430

Abstract

The NBU air shower array consisting of 21 plastic scintillation detectors has been operated in conjunction with two shielded muon magnetic spectrographs (m.d.m.~500 GeV/c) for more than one year now. The energy spectra in the range 2 GeV to 400 GeV of muons recorded by the spectrographs in air showers of size 10**4 to 10**6 have been determined as a function of muon lateral position from the air shower axis. The spectral results are presented along with theoretical comparisons.

1. Introduction. The NBU air shower array of 21 scintillation detectors covering an area of 1200 sq.m. has been operated in conjunction with two shielded muon magnetic spectrographs (m.d.m.~ 500 GeV/c). The array described by Basak et al/1/ has a layout of detectors in square symmetry set up on the ground level around two magnetic spectrograph units (height~7 m). The array with core location accuracy within $\pm$ 1 m and the shower size accuracy within $\pm$ 10-15% is sensitive to showers in the size range 10**4 to 10**6 particles. It was designed to detect muons of different energies simultaneously by two magnetic spectrographs installed at a separation of 4 m. A shielded neon flash tube chamber (height~1 m) at a distance 3 m from the spectrographs was operated for the detection of low energy muons.

2. Experiment. The air showers were detected by trigering any three of the seven detectors set up for coincidence at the array centre. Shower data at each triggering of the array have been recorded on a paper tape by means of a line printer and the spectrograph data for muon trajectory were recorded on a 35 mm film by a photographic arrangement/2/.

3. Method of analysis. All the recorded shower data were analysed on the basis of standard least-squares programme using Hillas structure function. The muon record on the film was first magnified to near actual size and then actual trajectory of the muon determined for the purpose of calculating momentum within the track location accuracy $\pm$ 0.19 cm.

For vertically incident showers, the average muon density as a function of muon position in a shower was determined out to 120 m from the shower core for each of 4 small shower groups in the range 10**4 to 10**6 of shower size. For each shower group, the measured momenta of muons distributed in 12 distance groups were converted to energies and corrected for energy loss in solid iron magnet and spectrograph shield which together sets a cut off at~2.5 GeV for muon detection by the spectrographs.

4. Results. For each shower group, the integral energy spectra obtained for 5 distance bins, 0-7.5m, 7.5-15m, 15-30m, 30-60m and 60-120m are given in figure 1-4. A representative set of our data with a sample from the work on EAS muons of MSU group/3/ is given in talbe 1 for comparison. In addition, the calculations of Greisen/4/ and of Khrenov and Linsley/5/ on EAS muons as a function of energy and distance were considered for comparison. Our measured distributions are flatter than the Greisen distributions. The distribution of Linsley is in agreement with our distributions over the range of energy and lateral distances studied in the present experiment.

Table 1

Present Experiment $\bar{N}_e = 3.34\times10^5$ $\bar{r}$ =25.37 m		MSU group[3] data $\bar{N}_e = 4.2\times10^5$ $\bar{r}$ =23.1 m		Present Experiment $\bar{N}_e = 9.57\times10^5$ $\bar{r}$ =42.41 m		MSU group[3] data $\bar{N}_e = 9.5\times10^5$ $\bar{r}$ =44.2 m	
$>E_\mu$ in GeV	ρ_μ in m^{-2}	$>E_\mu$ in GeV	ρ_μ in m^{-2}	$>E_\mu$ in GeV	ρ_μ in m^{-2}	$>E_\mu$ in GeV	ρ_μ in m^{-2}
10.0	0.35	10	0.76	10.0	0.410	10	0.40
53.7	0.13	50	0.28	53.7	0.097	50	0.12
113.3	0.05	100	0.15	113.3	0.031	100	0.033
204.0	0.02	200	0.048	204.0	0.0051	200	0.007

A selection of data at four different muon energies, 2.5 GeV, 11.3 GeV, 25.5 GeV, 53.7 GeV for each of four shower groups is presented in figure 5-8 to show the trend of distribution of muons in various distance groups. The observed distributions with considerable statistical errors at large distances show a close fit to the solid curves which are a plot of a standard function of the form $\rho_\mu = Ar^{-\alpha}\exp(-r/r_o)$ to indicate the trend of the lateral distribution at various muon threshold energies. Figure 9 shows the radial distributions for muons of threshold energy 25.5 GeV for all four shower groups.

5. Discussion. The initial analysis given in this paper using a sample of 1200 muons only has given an orientation to study all the aspects of muons on the basis of Monte Carlo simulation of air showers. The work on simulation programme is in progress now.

6. Acknowledgement. The financial assistance granted by Department of Atomic Energy, Government of India for this work is gratefully acknowledged.

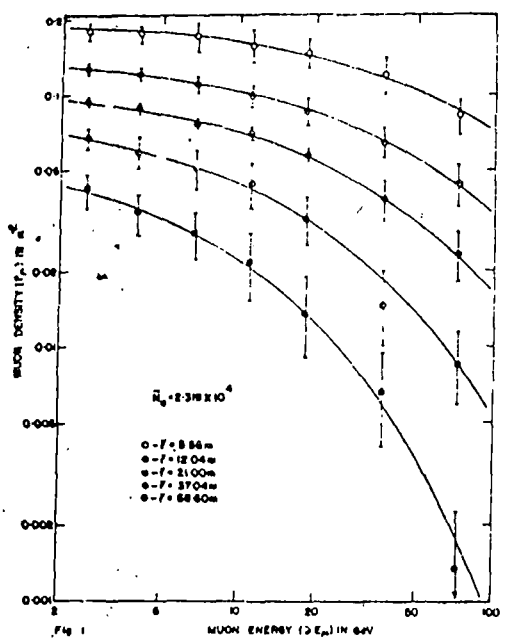

Fig 1

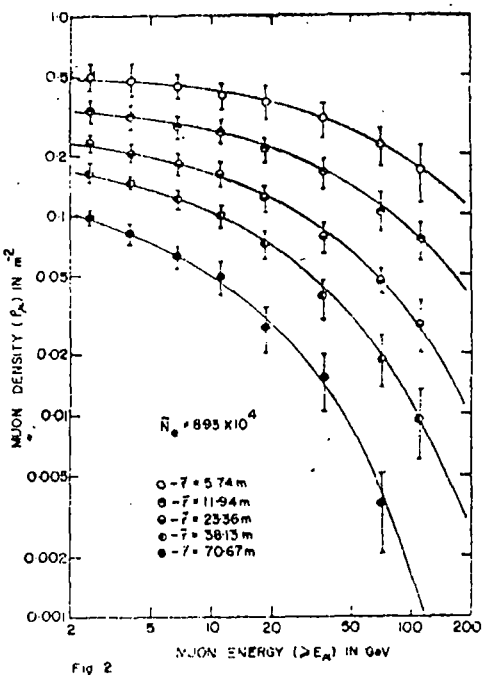

Fig 2

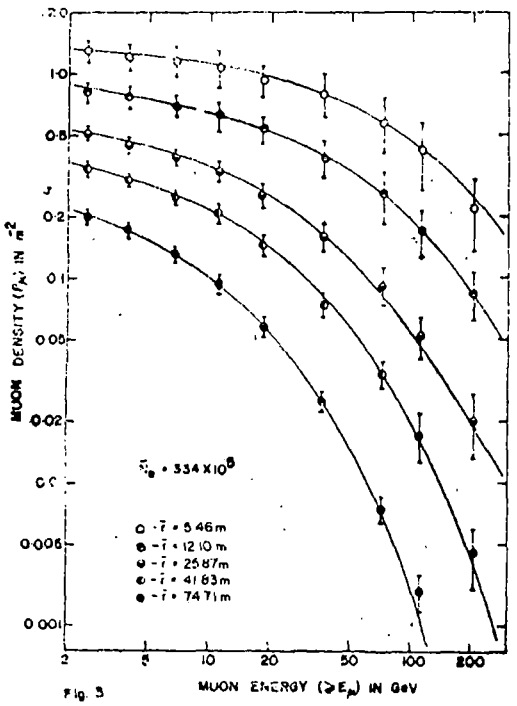

Fig. 3

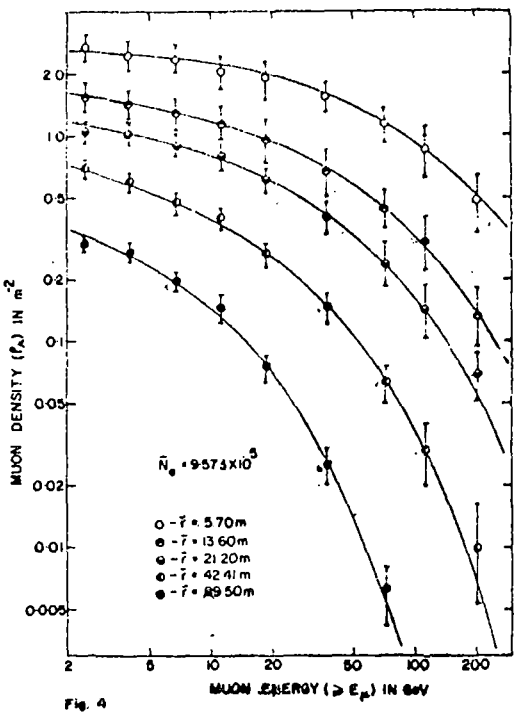

Fig. 4

Fig. 1—4. Muon energy spectra at various shower sizes in different distance bins. Solid lines are from the result of Khrenov & Linsley(5) distribution function

References

/1/ Basak, D.K., et al., Nucl.Inst.Meth.,227(1984)157.
/2/ Goswami, G.C., Ph.D. Thesis, North Bengal University, 1983.
/3/ Atrashkevich, V.B. et al., 18th.ICRC,Bangalore, 11(1983)229.
/4/ Greisen, K., Ann.Rev.Nucl. Sci., 10(1960)63.
/5/ Khrenov, B.A. and Linsley, J., 17th.ICRC,Paris, 10(1986)354.

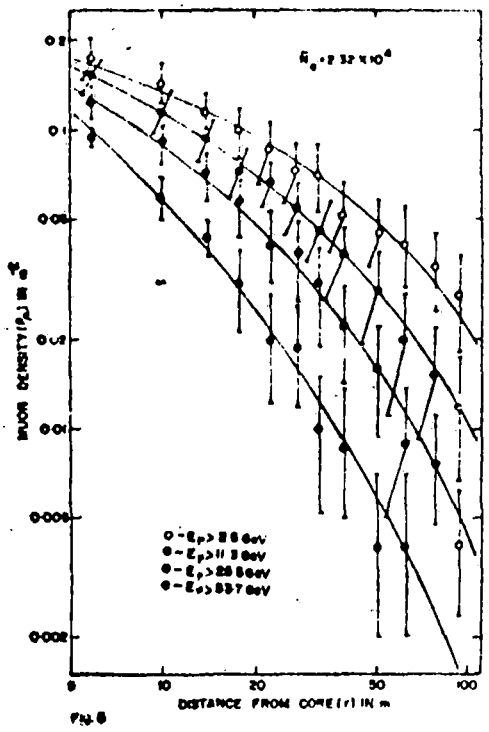

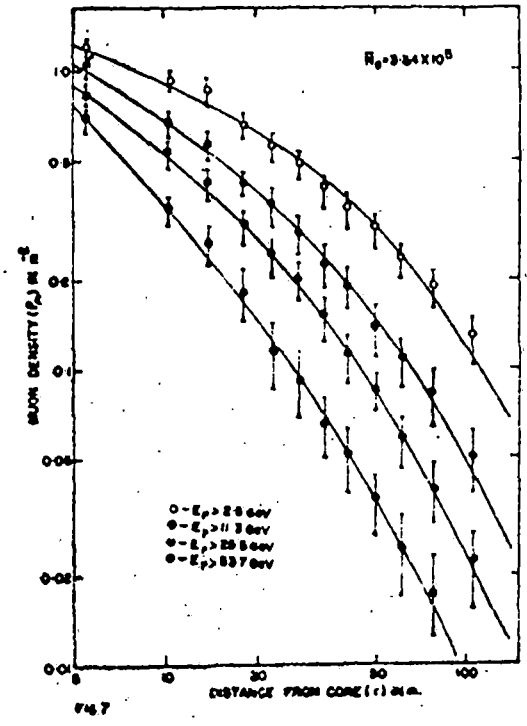

Fig.5-8. Lateral distribution of muons at various shower sizes for different energy threshold of muon. Solid lines are the best fit to the data.

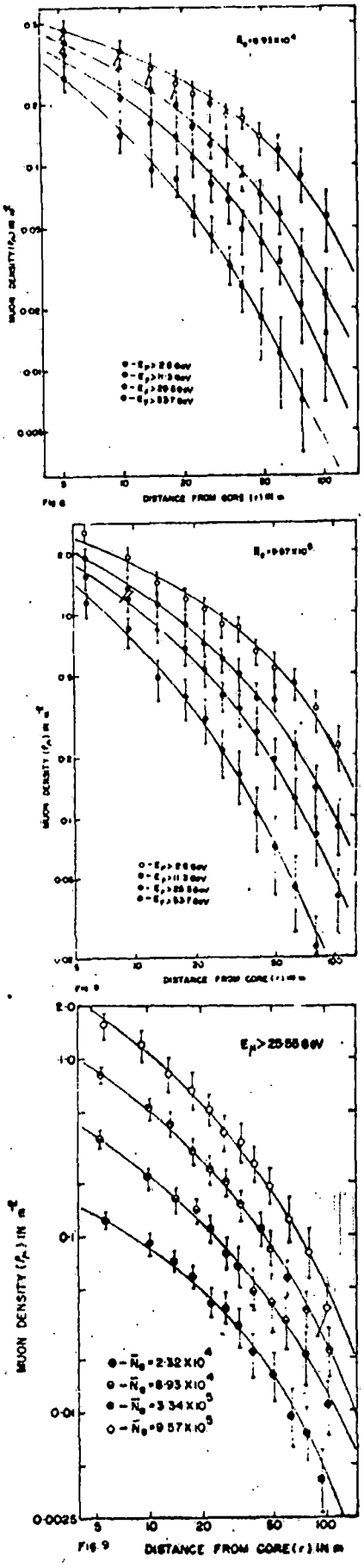

Fig.9. Lateral distribution of muons at energy threshold 25.5 GeV for different shower sizes.

PRIMARY COMPOSITION OF COSMIC RAYS FROM EAS MEASUREMENTS

Samir Kumar Sarkar, Narendra Nath Mukherjee, Mihir Kumar Roy
Bhaskar Bhattacharyya, Nripati Chakraborty and Nirmalendu Chaudhuri

High Energy Cosmic Ray Centre, University of North Bengal, North Bengal University (NBU) Dist.Darjeeling, India-734430

Abstract

Air showers in the size range 10**4 to 10**6 have been recorded by the NBU air shower array to detect muons of different energies in these showers by two shielded muon magnetic spectrographs (m.d.m.~500 GeV/c). The muon size as a function of shower size has been obtained for different muon threshold energies from 2 GeV to 54 GeV. The results have been utilized to infer the primary composition using the calculations of other groups. The electron and muon sizes have been used to deduce the primary integral flux in the energy range 5.10**13 to 2.10**15 eV. The integral flux points from the measured EAS muon spectra are in excellent agreement with direct measurements (12th.ICRC,1971).

1. Introduction. The muon size in various air shower size groups in the range 10**4 - 10**6 particles have been determined by experiments using the NBU air shower array which includes 21 scintillation detectors and two shielded muon magnetic spectrographs (m.d.m.~500 GeV/c). Details of the array and the spectrographs have been described in our earlier publication/1/. The NBU array having a square symmetry in detector location has a shower core location accuracy within ± 1 m and the shower size measurement accuracy within 10 - 15%.

2. Experiment. With two magnetic spectrographs each of two limbs to detect simultaneously muons of different energies in individual shower and a shielded neon flash tube chamber as the third low energy muon detector, the muons could be detected at five different locations in a shower. By using small area (0.25 sq.m) electron detectors at separation of 8 m, the electron structure could be resolved in individual showers out to 120 m. The information on muon trajectory through spectrograph was photographed by a set of camera/2/ and the shower data were recorded on a paper tape. The vertical incident showers with ~90% efficiency of array have been included for the measurement of flux.

3. Method of analysis. In the initial analysis, the showers in the size range 10**4 - 10**6 have been devided into 7 groups with the size bin (1-2).10**4, (2-4).10**4, (4-8).10**4, (8-16).10**4, (1.6-3.2).10**5, (3.2-6.4).10**5 and (6.4-12).10**5. Each shower group was again subdivided into 12 radial groups such that the smallest one had a width of 4 m. For each of several muon threshold energies in a shower group, muons were distributed into the 12 radial bins to determine the muon average radial positions out to a distance 120m. These distributions have finally been integrated to obtain muon number for each of different thresholds and hence the muon size for the threshold 2.5 GeV was determined. The electron size in the shower was determined by the

standard least-squares programme using Hillas structure function.

Primary energy of each shower was determined both from electron size and muon size using Monte Carlo simulation results /3,4/.

4. Results. The corelation between the electron size and the muon size for each threshold was examined by a connecting formula of the form $N\mu = A(N_e/10^{**4})^{\alpha}$ using least-squares method. The straight lines in the figure 1 show this connection for four different muon thresholds. The error bars to the experimental points are purely statistical. In figure 2, the plot, at 10 GeV muon threshold, for N_e vs. N_μ is shown with the results of a calculation/5/ on the connection between N_e and N_μ for various primary mass number. In addition, we have given below (Table 1) a comparison of our results with those obtained by Monte Carlo simulation/6/.

The primary energy spectrum derived from the electron size data is shown in figure 3 and that derived from muon size data is shown in figure 4. A comparison is given in figure 5 with the direct measurements of integral flux to demonstrate the accuracy of the present air shower experiment.

Table 1

Present Experiment of NBU Array $E_\mu > 2.5$ GeV			Monte Carlo simulation[6] $E_\mu > 2$ GeV (Proton primary)		
E_o in eV	N_e	N_μ	E_o in eV	N_e	N_μ
9.38×10^{13}	1.53×10^{4}	1.11×10^{3}	1×10^{14}	1.08×10^{4}	1.55×10^{3}
4.91×10^{14}	1.18×10^{5}	4.25×10^{3}	5×10^{14}	8.8×10^{4}	6.6×10^{3}
1.50×10^{15}	4.67×10^{5}	9.81×10^{3}			
			2×10^{15}	5.39×10^{5}	2.24×10^{4}
2.67×10^{15}	9.57×10^{5}	1.60×10^{4}			

5. Discussion. The comparison of our results on muon number ($E_\mu > 2.5$ GeV) with those for muons ($E_\mu > 2$ GeV) from Monte Carlo calculation of Wrotniak and Yodh/6/ and with the calculation of Antonov et al/5/ on additive quark model has set a level of confidence in the exercise of extracting primary composition from air shower observations.

The integral energy spectrum of Grigorov et al/7/ is in better agreement with the spectrum derived from the muon sizes. These results are based on calculation of other workers. Our own Monte Carlo programme has been in progress now.

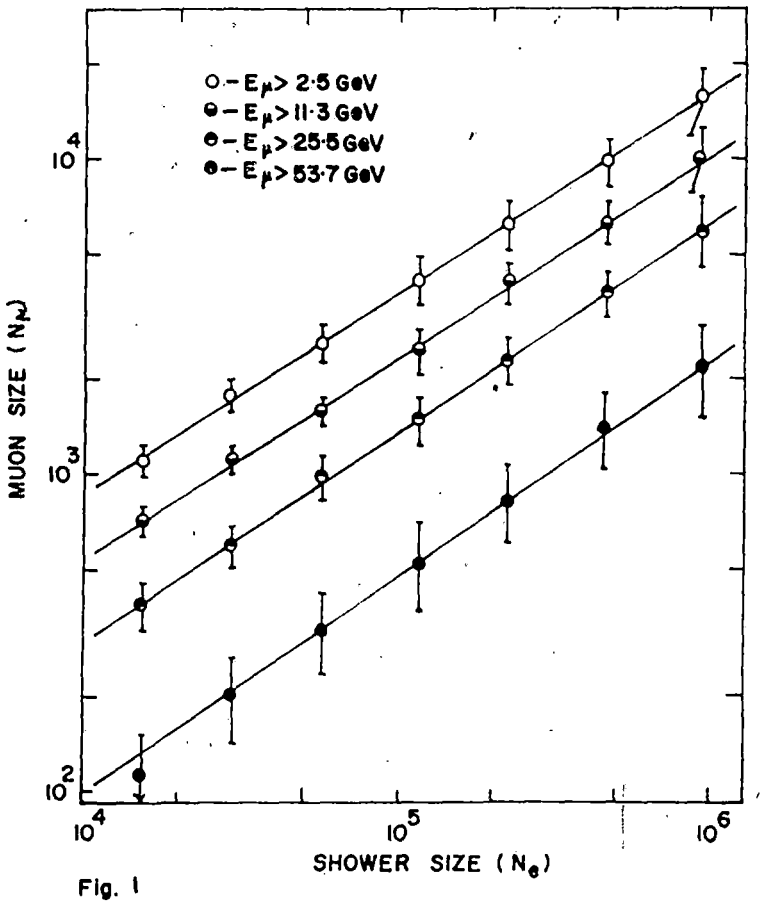

Fig. 1

Fig.1. Variation of muon size with shower size for different muon energy threshold.

6. Acknowledgement. Financial support from the Department of Atomic Energy, Government of India is thankfully acknowledged.

References.

1. Basak, D.K. et al., Nucl.Inst.Meth. 227(1984)167.
2. Goswami, G.C., Ph.D. Thesis, North Bengal University, India, 1983.
3. Rao, Srikantho, Ph.D. Thesis, TIFR, Bombay, India, 1981.
4. Giler, M. et al., Proc. 11th.ICRC, Budapest, 3(1969)549.
5. Antonov, R.A. et al., Proc. 18th.ICRC, Bangalore, 5(1983)159.
6. Wrotniak, J.A. et al., Proc. 19th.ICRC, La-Jolla, 7(1985)1.
7. Grigorov, N.L. et al., Proc. 12th.ICRC, Hobart, 5(1971)1746.

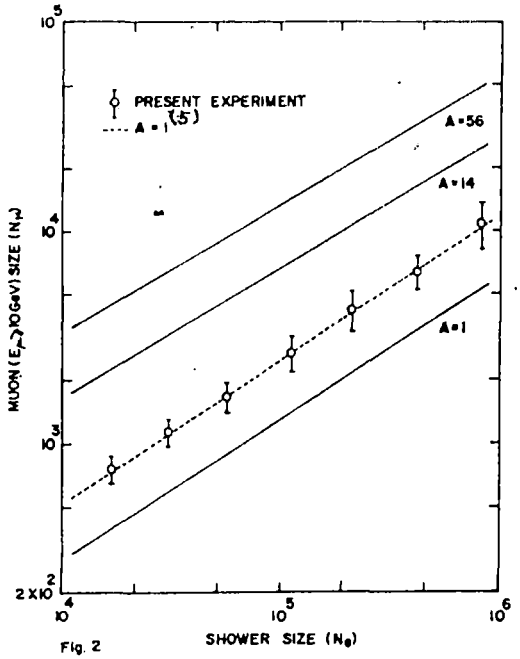

Fig. 2

Variation of muon size with shower size for muon energy threshold 10 GeV (comparison of present result with other[5]).

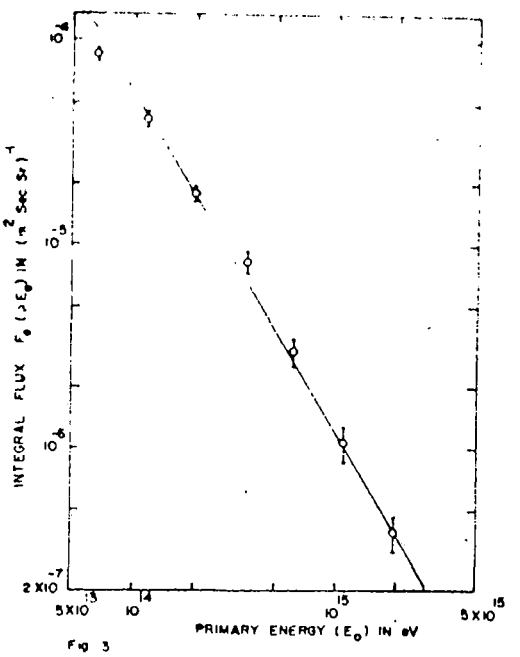

Fig 3

Integral energy spectrum of primary from electron-sizes.

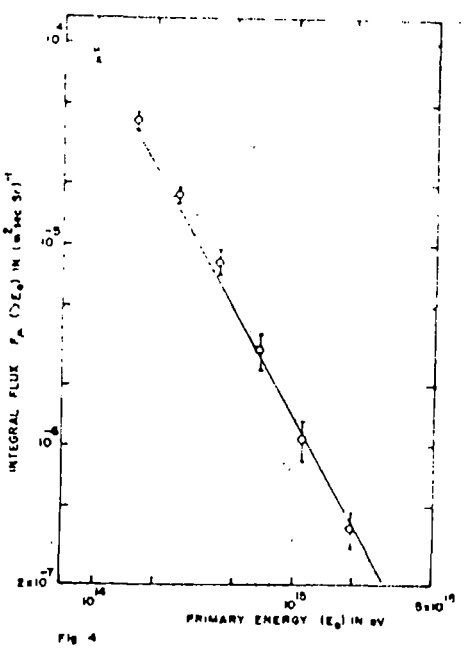

Fig 4

Integral energy spectrum of primary from muon-sizes.

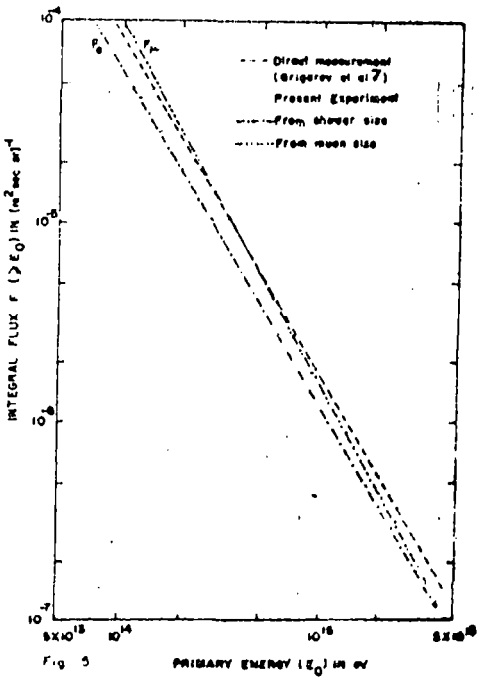

Fig 5

Comparison of the integral energy spectra of primary from electron-sizes and from muon-sizes that with the direct measurements[7].